COO-2233-2

INFRARED EMISSION AND 10.6 μm. LASER SCATTERING FROM THE DENSE PLASMA FOCUS

by

Richard S. Post

1973

Plasma Laboratory

Report No. 59

School of Engineering and Applied Science

Columbia University

New York, N.Y. 10027

This research was supported by the National Science Foundation Grant NSF GK-26326 and the U.S. Atomic Energy Commission Contract No. AT(11-1)2233.

DISCLAIMER

ABSTRACT

An experimental study has been conducted on a dense plasma focus using CO_2 laser scattering and infrared bremsstrahlung emission along with the standard diagnostics of neutron, hard and soft x-ray emissions, streak and framing photography. These diagnostics help demonstrate a two stage development of the plasma: a high density pinch stage followed by a lower density turbulent stage. Both stages are found to contain local sources of strong nonthermal, infrared emission with enhancements upto 10^6 over thermal bremsstrahlung levels. During the pinch phase the nonthermal radiation has frequency $\sim 2\omega_p$. During the low density stage, nonthermal radiation is observed at a frequency many times higher than the average plasma frequency and it is postulated that small current filaments (plasmoids) form which have density ten times larger than the average plasma density. CO_2 laser backscattering experiments failed to give positive results, thereby indicating turbulent levels of $S(k) \leq 2 \times 10^3$, $k \sim 1\mu^{-1}$, averaged over the scattering volume ($\sim 10^{-1} cm^3$). However, large $S(k=1\mu^{-1})$ could occur in local regions characteristic of the IR source dimensions ($\sim 10^{-4} cm^3$).

ACKNOWLEDGEMENT

I would like to thank my advisor, Professor T.C. Marshall for his help and guidance and stimulating discussion during the course of this work. The interest and encouragement of Professor R.A. Gross is sincerely appreciated.

Special thanks to Don McNeill for helping build the focus and performing many of the measurements and to H.C. Lui for the use of his computational calculations of the plasma focus. No one does an experimental thesis alone and it is the many unseen hands that made this experiment possible. I would like to thank Moe Cea, Hector Urbina and Don Osias for the help they gave me in the Plasma Lab. The constant repairs of the oscilloscopes by Tony Novinsky's electronic shop is appreciated. Thanks to Ralph Albertson for making numerous pyrex insulators under duress and to John Osarczuk and Paul May for machining the parts for the plasma focus.

Thanks also to Mary Black for typing the thesis and to Lorraine Mont who has promised to deposit it. Most of all I'd like to thank my friends here for the many chess games and B.S. which made my stay here so enjoyable and to my wife, Janet, for everything.

TABLE OF CONTENTS

		Page
ABSTRACT		i
1.	INTRODUCTION	1
	1.1 The Dense Plasma Focus	1
	1.2 Objectives of this Study: IR Radiation and Scattering	5
2.	EXPERIMENTAL METHODS	11
	2.1 The Plasma Focus Device	11
	2.2 Diagnostic Methods	17
	2.2.1 Terminal Characteristics	17
	2.2.2 Visible Light Photography	18
	2.2.3 X-ray and Neutron Measurements	19
	2.3 Infrared System	21
	2.3.1 Infrared Detector	21
	2.3.2 Spectral Analysis	24
	2.3.3 Optical System	25
	2.3.4 Laser	28
3.	PRESENTATION OF DATA	31
	3.1 Terminal Characteristics	31
	3.2 Visible Light Photographs	33
	3.3 X-rays and Neutrons	36
	3.4 Infrared Bremsstrahlung	38
	3.5 Laser Measurements	47
	3.6 Discussion of Laser Measurements	49
	3.6.1 Reflection	50
	3.6.2 Refracted Signal	52
	3.6.3 Incoherent Scattering	53
4.	DISCUSSION OF DATA	56
	4.1 Focus Plasma State	56

		Page
4.1.1	Review of the Relevant Results from Peacock	56
4.1.2	Estimation of Plasma Parameter During Pinch Phase	57
4.1.3	Possibility of Beams in the Focus	59
4.2	Discussion of the IR Radiation	60
4.2.1	IR Data from 1.6 Torr Experiments	61
4.2.2	IR Data from 1.1 Torr Experiments	67
4.3	CONCLUSION	70
	APPENDIX	73
	REFERENCES	76

1. INTRODUCTION

This work presents results of an experimental study on a fast pulse discharge usually referred to as dense plasma focus (DPF) or simply plasma focus. In this study we have examined the free-free bremsstrahlung near the plasma frequency and have looked for collective backscattering from long wavelength fluctuations ($\lambda >> \lambda_D$). Both of these measurements yielded information on the collective behavior of the discharge.

1.1 THE DENSE PLASMA FOCUS

The plasma focus has been studied for the past ten years in the U.S.[1] and abroad.[2] Interest in the plasma focus has been generated by the fact that for many years it was the densest, high-energy, laboratory-produced plasma. Temperatures on the order of 1 keV and density $\sim 10^{19}/cm^3$ are obtained with the DPF and neutron bursts $\sim 10^9$ to 10^{11} which last $\sim$ 100 nsec. can be generated in a deuterium plasma.

Although the plasma focus has been studied for some time, a detailed theoretical understanding has not yet developed. This is a result of the attainment of high energy density in times comparable to equilibrations times for plasma constituents and two-stage characteristic of the plasma focus, i.e., a pinch phase followed by a lower density phase. Detailed experimental work has been further complicated by the

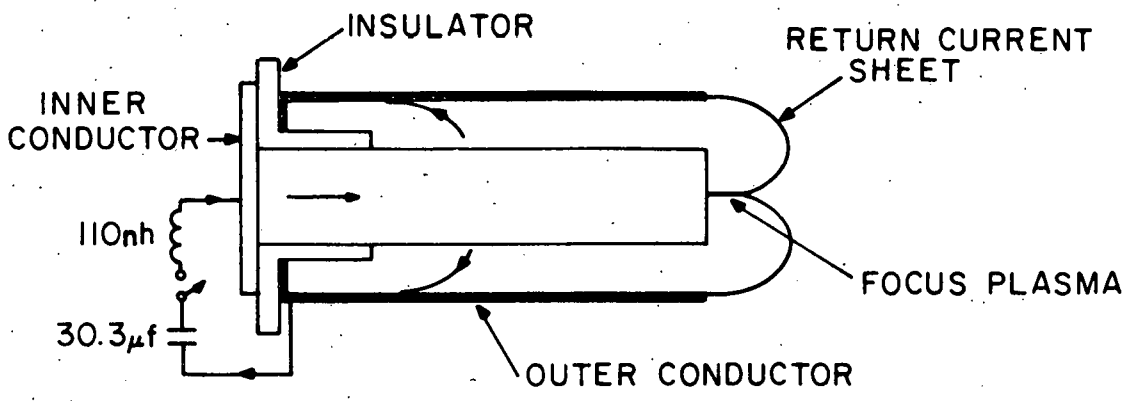

Figure 1-1: Schematic of the plasma focus with solid inner conductor. After breakdown along the insulator, the current sheet propagates in the space between inner and outer conductors. Arrows indicate current flow as the current sheet is accelerated towards the end of the electrodes. Later in time, at current maximum, the plasma focus is formed off the end of the inner conductor.

short duration (~ 200 nsec.) of the plasma, its small size ($\sim 5 \times 10^{-2}$ cm^3), high temperature and large variations in plasma characteristics from shot to shot.

We will describe the dynamics of the focus and discuss some of the results obtained from experiments in other laboratories to lay a foundation on which to present our work. However, exact carry-over of data, such as density, temperatures, etc., from one experiment to another is not possible since different apparatus vary in operating filling pressure, bank energy, etc.

The plasma focus operates by passing a capacitive discharge between coaxial cylinders in hydrogen or deuterium at ~ 2 torr (fig.1.1). The current is accelerated by the $\underline{J} \times \underline{B}$ force and propagates in the axial direction. In about 3 μsec. the current sheet reaches the end of the inner cylinder at current maximum (3.2×10^5 Amps.). The current sheet, as it rolls over the end of the center electrode, forms a quasi-cylindrical collapse, which is accelerated towards the axis by a rapidly increasing magnetic force ($B \sim \frac{1}{2}$ Mgauss). The collapse time is ~ 100 ns during which the current is approximately constant. Therefore, $\underline{J} \times \underline{B} \propto \left(\frac{I}{r}\right)^2$ increases rapidly as r decreases from 25 mm. to 1 mm. (the final radius).

The dynamic motion of the current sheet can be seen in computer plots of the temperature profile (fig.1.2) from a 2-dimensional single fluid code which was lent to us by H.C. Lui.*

This shows the important dynamics of the focus beginning during the quasi-cylindrical collapse. The time prior to

* Private communication, H.C. Lui, doctoral student, Plasma Physics Laboratory, Columbia University.

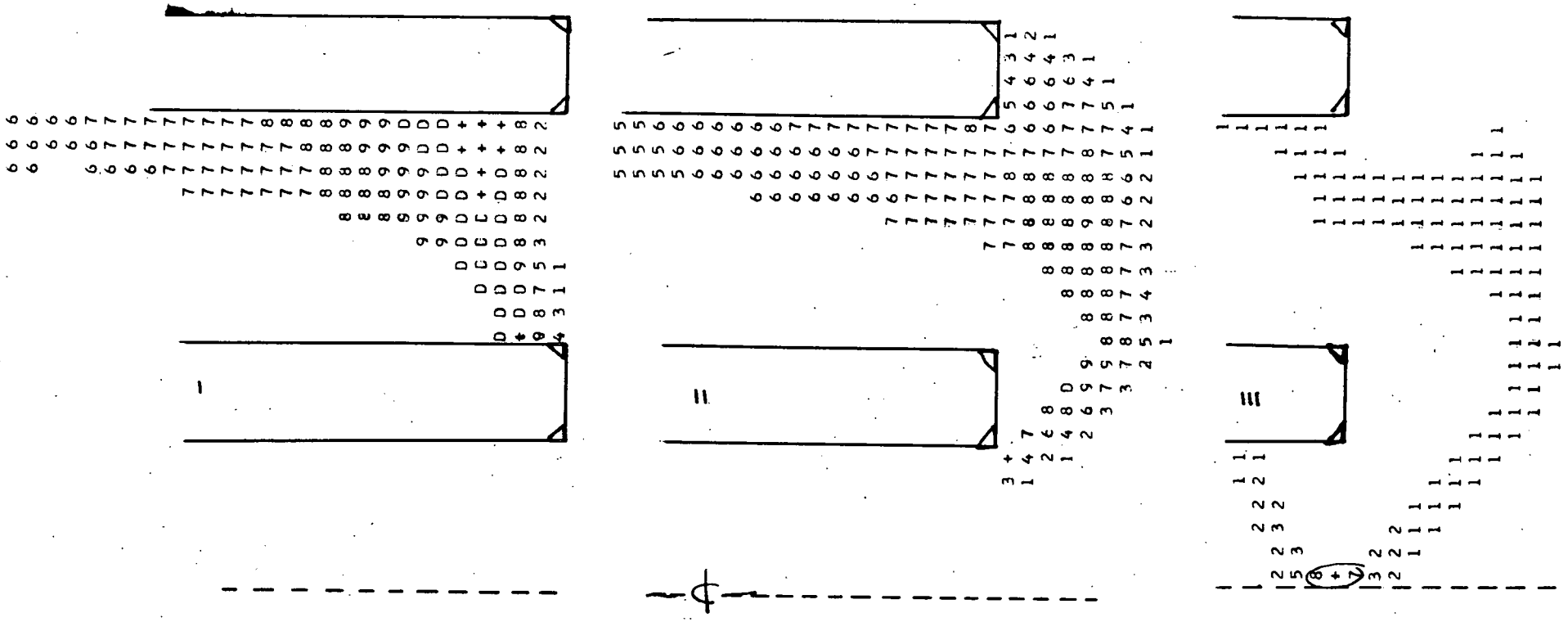

FIGURE 1-2

TEMPERATURE CONTOURS COMPUTED FOR 1.1 TORR D_2 WITH I_P = 500 KA. I SHOWS CURRENT SHEET PROPAGATING; II SHOWS COLLAPSE STAGE; III SHOWS FORMATION OF PINCH. TEMPERATURE SCALE IS DIFFERENT FOR EACH PLOT. MAXIMUM TEMPERATURE ($T_E + T_I$) = 1.5 KEV. DURING PINCH (+). OUTLINED AREAS ARE CONDUCTOR SURFACES.

arrival of the current sheet at the end of the center electrode serves only to allow the capacitor bank to build up to maximum current. As can be seen in Fig.2 the current sheet has velocity in both the radial and axial directions. This axial velocity allows the escape of most of the particles ahead of the sheet. The magnetic field compresses only ~ 15% of the particles initially ahead of the collapsing sheet.[3] This fact permits a smaller final plasma radius and hence larger magnetic compression and energy density than one would have obtained in a purely cylindrical collapse. We obtain a plasma with bulk properties estimated* to be $n_e \sim 3 \times 10^{18}/cm^3$, $Te \sim 750$ eV, $Ti \sim 250$ eV for a deuterium plasma of ~1.5 mm. in radius and ~ 1.5 cm. long. At this time the focus is in its dense pinch phase. The plasma volume contains ~ 25 J of thermal energy and is a copious source of x-rays and neutrons.

The density and size of the dense pinch phase can best be studied by taking shadow and interferograms. Such data has been obtained by Peacock[4] on a larger focus using a 1 ns ruby laser pulse. His photographs show a pinch which is Rayleigh-Taylor unstable with growth rates ~ 10 ns. The pinch column lasts for ~ 40 ns. and finally pinches off in an m=0 mode. Before pinching off he finds the average density is $\sim 6 \times 10^{18}/cm^3$ with peak density $\sim 4 \times 10^{19}/cm^3$ in the most tightly pinched regions. After the dense pinch breaks off, a less dense plasma forms with density $\sim 10^{18}/cm$. In the low density phase, the plasma continues to emit neutrons at the same rate as in the dense pinch stage. The density and temperature of the dense stage are

* See section 4.1.2

well predicted (within a factor of 2)[4] from Potter's 2D, two fluid numerical code;[3] however, the following low density stage is not obtained and the neutron yield predicted by the code is too low.[3,4]

The neutron and x-ray emissions of the plasma focus have interesting features not characteristic of a Maxwellian plasma. The D-D neutrons emitted in the axial direction were shown by Bernstein[5] et al. to have an average shift of 500 kV in the axial direction and an anisotropy of 11% in the forward direction. It has been suggested that accelerated ions in the $\underline{B}_\theta \times \underline{E}_z$ fields could account for such observations.[5]

Simultaneous with the start of neutron emission is the emission of hard x-rays (> 80 keV) which have a quadrupole distribution about the axis.[6] The duration of the hard x-rays is about equal to that of the dense pinch phase. The time integrated hard x-ray distribution measured by van Paasen[7] gives an energy distribution of hard x-rays from 60 keV. to 500 keV. which can be described by a function $\frac{1}{E}\frac{dN}{dE} = A\,E^{-2.5}$ for both a large (336 μf bank) and small (84 μf bank) machine. The soft x-ray spectra show similar power law distributions as opposed to $e^{-h\nu}/KT$ as given by a Maxwellian plasma. Typically, only 20 to 30 kV are applied to the devices but large potentials are induced by the rapid change in inductance associated with the pinching column $\left(\text{i.e. } V \propto I\frac{dL}{dt}\right)$. However, it is not clear that these high voltages are associated with the hard x-rays.

Further interesting features of the soft x-ray spectra ≤ 10 keV. are seen in time-integrated x-ray pinhole photographs.

Such photographs[8] show small (< 0.1 mm.) intense x-ray sources located within the pinch column which do not emit isotropically. Filamentary shapes have dimensions smaller than the pinch column.

Our work did not attempt to reproduce all of the work cited above, but enough data on neutrons and x-rays was taken to make comparisons with the work of others and also to monitor the functioning of the apparatus.

1.2 OBJECTIVES OF THIS STUDY: IR RADIATION AND SCATTERING

Our program of research was to investigate the DPF using techniques of CO_2 laser scattering and infrared bremsstrahlung. A salt prism spectrograph or narrow filters served both to measure the bremsstrahlung and to analyze the scattered spectra. These details are given in Chapter 2. Initial measurements perpendicular to the axis showed that the cool gas which carries the return current is very lossy. Transmission measurements through the return current sheet using 10.6μ radiation from a CO_2 laser showed an attenuation of $\sim$ 90% on a double pass through this gas. This led us to make measurements along the axis of the center electrode, thereby exposing the plasma focus region with little intervening cool plasma (see figure 2) and at the same time increasing the volume of focus plasma viewed by the detector.

Infrared bremsstrahlung provides several types of useful information. For frequencies greater than $3\omega_{pe}$ the radiation

is from coulomb scattering of electrons on ions involving small momentum change and is thus determined by the bulk of the particles rather than by a non-Maxwellian tail on the distribution function. (On the other hand, such energetic particles have a large influence in the x-ray bremsstrahlung.) As $I(\omega)\,\Delta\omega \propto n_e^2\, T_e^{-\frac{1}{2}}\,\Delta\omega$, the radiation gives an approximate time history of n_e (t) due to the weak dependence on T_e. As one continues to measure bremsstrahlung at lower frequencies near $2\omega_{pe}$ and ω_{pe}, enhanced bremsstrahlung may be observable through the radiation of plasma waves generated by fast electrons.[9,10] Such enhancements are believed responsible for type II and III solar radio bursts.[11]

Laser backscattering near the plasma frequency can be used for several types of measurements. If dense regions with $n_e > 10^{19}/cm^3$ exist in the plasma column, then these regions become totally reflecting regions for 10.6μ radiation, as the incident frequency is now equal to the plasma frequency. The density of the plasma focus has often been stated[5] to be as high as $10^{20}/cm^3$. If a region of the size of the plasma column having $n_e > 10^{19}/cm^3$ is accessible to the laser beam, then such a region backscatters 200 times the minimum detectable signal and should be observable even with sizable refractive loss. The time evolution of signals reflected from the critical surface would be interesting for studying the time evolution of the dense pinch.

For plasma with $\omega_{inc} < \omega_{pe}$, one can do collective backscattering from highly excited modes with a long wave length laser.

Radiation from a CO_2 laser (10.6μ) has $|\underline{k}| \sim 1/20\ |\underline{k}|$ of a ruby laser and therefore can be scattered from fluctuations with characteristic lengths much greater than the Debye length (collective modes) without resorting to small angle scattering. In fact, these scattering experiments detect collective modes in 180° back scatter. Due to the combination of low laser power, bremsstrahlung radiation and low sensitivity of infrared detectors, we were restricted to scattering from fluctuations greatly enhanced over thermal level; however, this is precisely what we are interested in studying for the following reasons:

One might expect to scatter from enhanced electron fluctuation during the dense pinch phase due to excitation from nonthermal particles. As we have $\omega_i \leq \omega_{pe}$, back scattered radiation from electron plasma fluctuations corresponds to a wave length $8\mu \leq \lambda \leq 5.3\mu$. The wave vector condition $\underline{k}_s - \underline{k}_i \cong \underline{k} \leq 3\underline{k}_i$, where $\underline{k}$ is the plasma fluctuation wave vector and s and i refer to the incident and scattered waves, implies

$$\frac{k}{k_D} \sim \frac{3k_i}{k_D} \sim \frac{3\omega_{pe}/c}{\omega_p/V_{th}} = \frac{3V_{th}}{c} << 1$$

Hence, the scattering is collective.[12] The form factor $S(k,\omega)$ which gives the departure from Thompson scattering due to spectra of the density fluctuation must be $S(k,\omega) \sim 10^4$ to override bremsstrahlung. Such enhancements are common for turbulent plasma.[13]

As the plasma pinches off, it has been proposed[14] that turbulent heating takes place. Since the neutron production remains high after pinch-off and the density has dropped by a factor of 10, some heating must take place. One should note that while the

plasma contains ~ 25 J of thermal energy, the adjacent 2 mm. contains 250J of magnetic energy. On expanding, the plasma occupies this volume and resistive dissipation of this field could provide a heating source. One mechanism suggested by Maissoner is the decay of vortices created by macroscopic turbulence generated by the pinching-off of the plasma. Such eddies then decay down to the scale of the ion cyclotron radius r_{ci} to $\sqrt{r_{ci} r_{ce}}$ characteristic of high β turbulence. These eddies are sufficiently small (size ~ skin depth) to dissipate the magnetic energy. Turbulence having this scale size should scatter the incident beam strongly since $r_{ci} \sim 40\,\mu$ for a 250 eV. deuteron, and $r_{ce} \sim 2\mu$ for a 750 eV electron in a $\frac{1}{2}$ Meggauss field, while the wave vector condition requires a scattering length of $\lambda \sim 5\mu$.

Another suggested[14] possibility is that microscopic turbulent heating takes place at some radius of expansion by a current-driven ion accoustic instability. Such instabilities have large S(k) for fluctuations with $k << k_D$ and are to be expected during the density decay. Taking $n_e \sim 10^{18}/cm^3$ and $T_e \sim 1$ keV gives $\lambda_D \sim 10^{-1}\mu$, and therefore, one expects scattering from modes with $\lambda \sim 200\lambda_D$. Such modes have been observed enhanced up to 10^4 over thermal levels in collisionless shock experiments.[16,17]

As can be seen from these estimates of scale size, the use of 10,6μ radiation in a backscatter experiment covers a number of different modes which may go unstable in the plasma focus. Successful backscatter will determine the existence of turbulence in the DPF.

2. EXPERIMENTAL METHODS

2.1 THE PLASMA FOCUS DEVICE

The plasma focus apparatus was designed to utilize an existing capacitor bank composed of 50 kV capacitors with a total capacitance of 30.3μf. The bank has a single trigatron spark gap and, including the one-foot parallel plate transmission line which connects to the focus, has a total inductance ~ 110 nh. This is a large inductance by plasma focus standards, but it is sufficiently low to deliver 320 KA. at current maximum to the plasma focus with the bank operating at 32 KV (stored energy 15.5 KJ.).

The entire apparatus can be seen in fig. 2-1. The electrode dimensions and insulator shape were obtained from machines built in other laboratories.[1] The only critical design parameters are the adjustment of the length of the inner conductor (so that the current sheet arrives at the end of the center electrode at current maximum) and the use of a launching insulator along the inner conductor, thus forming a parabolic-shaped current sheet. For the plasma focus to function properly, the pinch must form noncylindrically, and early work[1] has shown that this particular arrangement is satisfactory although other configurations have also been successful.[2,7]

The major problem in the design was a low inductance connection of the inner electrode to the parallel plate line, which would keep uniform stress on the pyrex insulator during

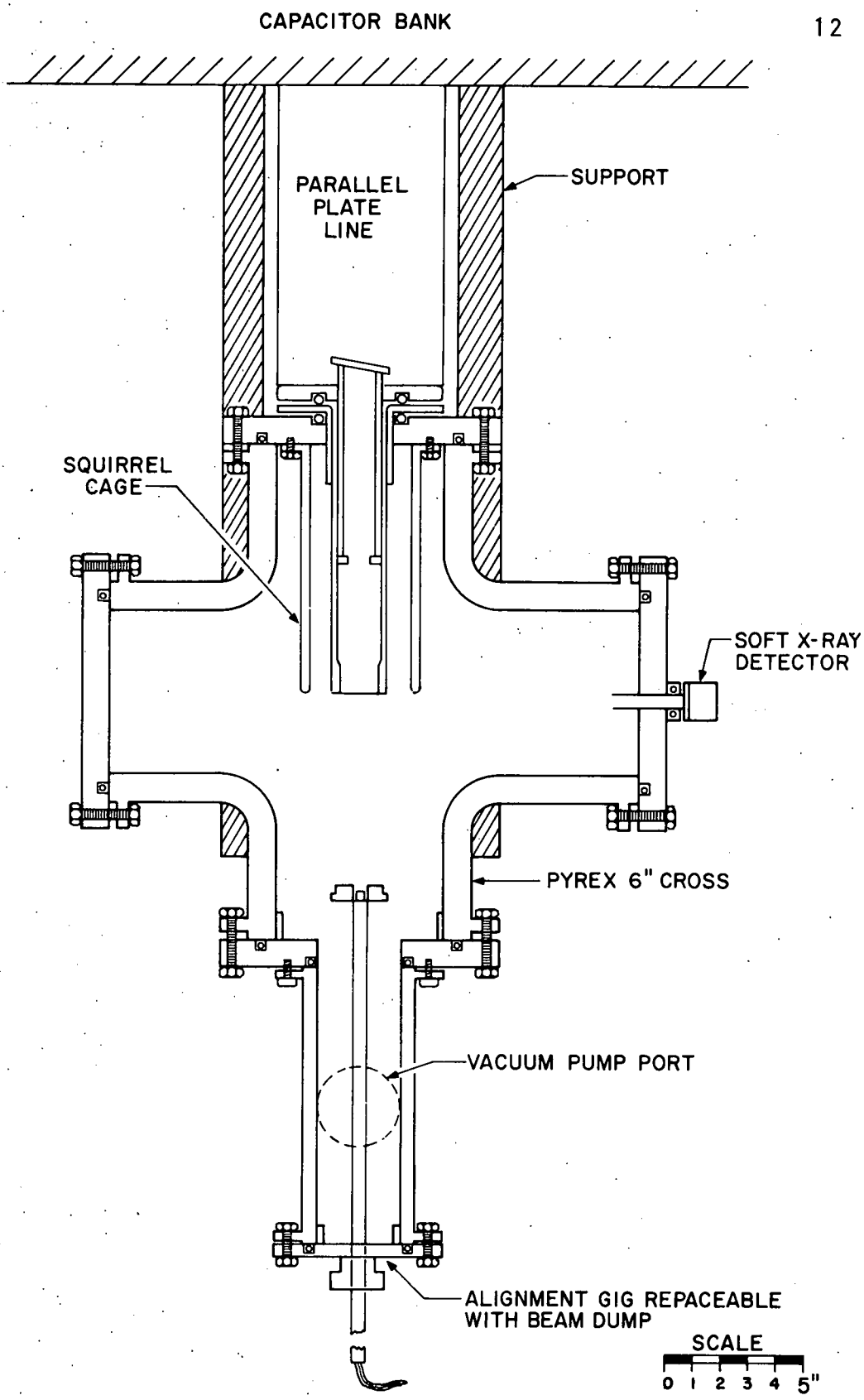

Figure 2.1 This drawing shows the plasma focus apparatus excluding the optical diagnostics.

the impulse of the discharge and also hold off the high voltage developed during the current sheet collapse (this voltage ranged up to 80 KV). This arrangement is shown enlarged in fig. 2-2. On several occasions an arc formed along the surface of the nylon insulator and cracked the pyrex insulator. On the next firing the full bank current would propagate through the crack and blow the insulator into powder.

When this tracking was identified, the air gap between the current carriers and dielectrics was filled with Dow Corning 4 compound, a high voltage silicon grease; after which, no further breakdowns occurred.

The focus was used with various outer and inner conductors. The outer conductor initially chosen was a solid tube, but it was soon replaced by eight rods forming a squirrel cage shown in fig. 2-1. The squirrel cage[17] allows the plasma flow to be pushed out of the magnetic field region so that the current sheet does not accelerate all the mass ahead of it. As a result, the focus can be operated at higher pressures for the same drive current. Also it was found that the current sheet arrival time to the end of the inner conductor was not very sensitive to filling pressure. For most of the work the filling pressure was 1.6 torr or 1.1 torr with a variation in arrival time of only 200 nsec.

Both a solid-faced and a hollow inner conductor were used in these experiments. The solid-faced inner conductor was used in initial experiments on laser absorption in the cool gas

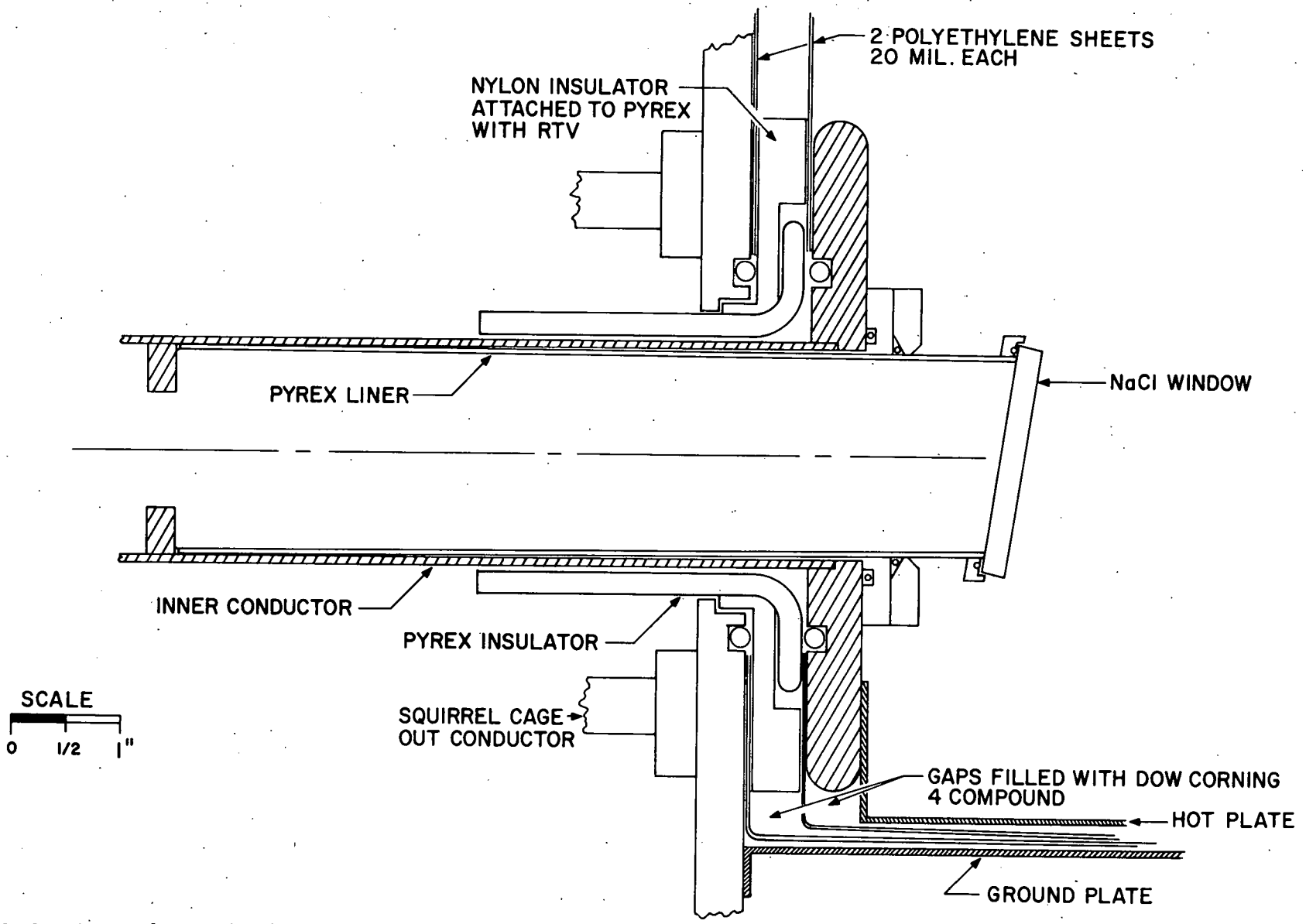

Figure 2.2 An enlarged view of the inner conductor showing high voltage insulation, pyrex launching insulator and high voltage connections. The NaCl window is mounted on a pyrex liner. The liner prevents arcs from occurring near the window.

region of the return current sheet and for image converter photographs. In order to gain optical access to the pinch without passing through cool gas, a hollow electrode was used. Such an arrangement was first used by Prior[18] to eliminate x-rays caused by anode bombardment. We found that use of the hollow electrode did not alter the focus behavior significantly. However, for reliable focussing,a few percent Argon had to be added to D_2 and the inner electrode had to be run positive.

A small percentage of Argon is widely used with deuterium chiefly because it was found empirically to increase neutron production and make the focus more reproducible. In the case of a hollow center electrode, the di/dt waveform shows only one spike during collapse, as opposed to multiple spikes seen with solid anodes;[19] the total neutron production and the x-rays of the dense pinch phase did not change substantially.

One precaution had to be taken in using the hollow anode. The pinch column squirts plasma in the axial direction all the way to the observation window at the end of the anode. This presents no problem during the time of measurements on the focus as it occurs microseconds after collapse. However, the plasma, on arrival at the window region, forms an arc which carries current through the anode interior and destroys the window surface by ablation and deposition of copper. This problem was handled by lining the inside of the anode with pyrex tubing which had the window mounted on the end of the tube. This device prevented arc formation near the window and removed the sputtering source to an iris located 20 cm. from the window. Even with this

arrangement, metal evaporation eventually reduced transmission through the salt window. After 20 firings of the focus a CO_2 10.6 μm. beam was attenuated by ~ 0.5.

The last significant problem was keeping the electrodes free of ablated material. Upon contact with such high energy plasma and large current, solid layers boil. The metal vapor and ablated glass did not seem to impair operation; however, o-rings, plexiglass or other similar materials would partly vaporize and deposit on the electrodes. As such deposits accumulate, the operation becomes erratic; i.e.,the current sheet arrival time varies and the amplitude of di/dt decreases. Small di/dt indicates failure to form a small pinch column (see section 2.2.1) and results in a low neutron yield. After this was recognized to be the cause of poor operation, all o-rings with direct access to the plasma flow were shielded by metal and no plastics were used where they might be exposed to the plasma. With these precautions the focus could be fired ~ 1000 times before cleaning became necessary. After a hundred shots electrodes appeared black from unknown deposits, but this did not affect operation.

The entire electrode arrangement used a Pyrex cross for a vacuum container. Vacuum requirements for the focus are modest since operating pressures are in the torr range. In general the machine was pumped down to 10^{-5} mm. for a few hours to outgas. A few shots were required after cleaning before the machine operated normally, a common feature of high current pulsed plasma machines.

During operation the machine was continuously pumped on

with a trapped roughing pump and during operation gas was leaked through a Veeco Leak valve. Argon was admitted to a pressure of $\sim 50\mu$, as measured by a Stokes gauge, and the balance of D_2 was added.

2.2 DIAGNOSTIC METHODS

2.2.1 TERMINAL CHARACTERISTICS

During the course of these experiments di/dt, i and V, the voltage across the breach of the focus, were measured. di/dt was obtained from a pick-up coil placed between the parallel plates at the connection to the focus. On every shot di/dt was measured as it served as a reference for the start of the pinch phase. This is understood from the fact that during the collapse, V x B at the current sheet becomes very large and reaches its maximum close to the axis where both V and B have their maxima. That di/dt is dominated by V x B of the pinch region is easily seen as the velocity of the current sheet towards the axis is $v \sim 50$ cm./μs at its peak, whereas $v \sim 10$ cm./μs for the remainder of the current sheet. The ratio of $\underline{B}_p$ of the pinch to $\underline{B}_s$ of the return current sheet is $\frac{B_p}{B_s} = \frac{r_p}{r_s} \sim \frac{1 \text{ mm.}}{100 \text{ mm.}}$ where r_p and r_s are the characteristic radii for the pinch and return current sheet. The ratio of the lengths of the pinch to return current sheet is $\sim 1/10$ so that $\left(\frac{di}{dt}\right)_{\text{pinch}} \Big/ \left(\frac{di}{dt}\right)_{\text{sheet}} \sim 50$. When the pinch forms on the axis, $V \longrightarrow 0$ and hence di/dt drops sharply (see fig. 3-1).

The focus current was obtained by integrating di/dt. A

calibration of i was obtained by shorting the inner to the outer electrode and ringing the bank at some known voltage.

With this data the integrated di/dt signal was calibrated and the current was measured for a given charging voltage. After that, the current itself was not measured; rather, the bank voltage was used to obtain the current. Since the bank inductance is large (~ 110 nH.), the current remains almost constant during collapse. The effect of bank inductance on circuits with variable inductance loads can be seen in calculations of Carpenter et al.[20]

The voltage across the breach was measured with the standard technique of a voltage divider using a $CuSO_4$ resistor[21] for the high voltage dropping resistor.

2.2.2 VISIBLE LIGHT PHOTOGRAPHY

Visible light streak and framing photographs were taken with an STL camera. Framing photographs were taken up the axis with the hollow electrode and perpendicular to the axis with a solid-faced electrode. Streak photos were taken only perpendicular to the axis with the solid electrode. In each case the focus region was imaged with a lens outside the vacuum system so that measuring scales or streak slits could be placed in the image plane. A framing photo gives three images of the emitted plasma light on a single firing of the focus. The duration was normally 10 nsec. with 50 nsec. separation between frames. The streak photos are made by imaging a slit, 1 mm. wide and placed at the

image plane of the focus, into the STL camera. The camera streaks this line image of plasma light across the photographic film in times as short as 500 nsec. The velocity of the light-emitting plasma can be measured in this way.

2.2.3 X-RAY AND NEUTRON MEASUREMENTS

Hard x-rays were measured by a 1" x 3/8" piece of Pilot B scintillator on a 6655A photomultiplier located in the screen room. The hard x-rays had to pass through the vacuum chamber (3/8" SiO_2) and 1/4" of Al which covered the scintillator as well as the 3.5 meter air path. The absorption of these materials[22] was estimated based on 2 cm. of Al. This absorption e-folds photons of energy less than 50 keV. As the spectrum is assumed to be falling off as the power law $\frac{1}{E}\frac{dN}{dE} = AE^{-2.5}$, the energy detected is $\sim$ 100 keV.

The soft x-ray spectrum was observed with a 2 mm. x 1/4" dia. plastic scintillator with a 1.5 mil. Al foil as a vacuum window. The energy band of this detector is defined at low energy by the 1.5 mil. Al window and at high energy by the thickness of the scintillator. Based on the mass absorption coefficient[23] for Al and a window thickness of 10 mg./cm.^{3}, one calculates less than e^{-1} absorption for photons of energy greater than 6 keV. The absorption coefficient for NE 102[24] gives absorption less than e^{-1} at 10 keV. These two energies define the bandwidth. In this band one is measuring continuum radiation involving free-bound transitions for an Argon-seeded plasma (appreciable line radiation from

Argon occurs for transition with energy less than 4 keV.)[25] No other soft x-ray bands were examined since, due to the nonthermal electron distribution,an electron temperature can not be measured by absorption foil techniques.

The light from the scintillator was coupled to a 931A PM through a metal light pipe made from polished stainless steel tubing. Standard fiber optics (both glass and plastic) were found to scintillate from the hard x-rays and were therefore useless. The use of a light pipe was dictated by the need to shield the PM from the hard x-ray flux by 2" of lead. Without such heavy shielding, the PM produced large dynode pulses in response to the hard x-rays.

The neutron flux was measured by observing the fast knock-out protons in a 2" dia. x 1" piece of Pilot B which was viewed by a 6655A PM. The detector was located in the screen room inside a lead house to shield it from the hard x-rays.

The voltage divider for the 931A was the standard high gain arrangement while the 6655A used a high current divider to insure linearity to high current pulses.[26] The 6655A PM divider used a zener between the cathode and first dynode to keep the transit time short and independent of the high voltage (this was varied to adjust the tube gain).

As the duration of the experiment is short and changing on a rapid time scale,the transit time of the PM's had to be measured to assure time correlation with other diagnostics. The transit time was measured with a light pulse obtained by charging

up the stray capacitance of a high pressure reed switch until the gap breaks down. The light pulse and simultaneous current pulse had a rise time of 5 nsec. and a half width of 10 nsec. Both the light pulses and a strobe with a light pulse of 800 nsec. were used to check the space charge saturation of the output pulse. During the course of experiments the tube gain was kept sufficiently low to insure good fidelity of the output pulse.

The total neutron flux was measured by standard silver activation foil techniques.[27] The counter was calibrated at Los Alamos and in our laboratory by D.H. McNeill.

2.3 INFRARED SYSTEM

2.3.1 INFRARED DETECTOR

The infrared detector was an Au doped Ge photoconductive detector operated at 77° K. It has peak responsivity from 2μ to 7μ and drops rapidly to 1/300 of its peak responsivity at 10,6μ; however, the detector is still usable at these longer wavelengths at reduced sensivity (see figure 2-3). At 75 V Bias and a load resistance of 500 Ω, the peak responsivity was 2.4 mV/mW at 4.5μ, falling to 8 mV/watt at 10.6μ. Five hundred ohms was the maximum load which could give satisfactory rise time (30 nsec.). The detector was also operated into 50 Ω to get minimum rise time (2 nsec.) at 1/10 the responsivity. Details of IR photoconductive detectors can be found in the literature.[28]

As IR signal levels were typically on the order of 10 mV,

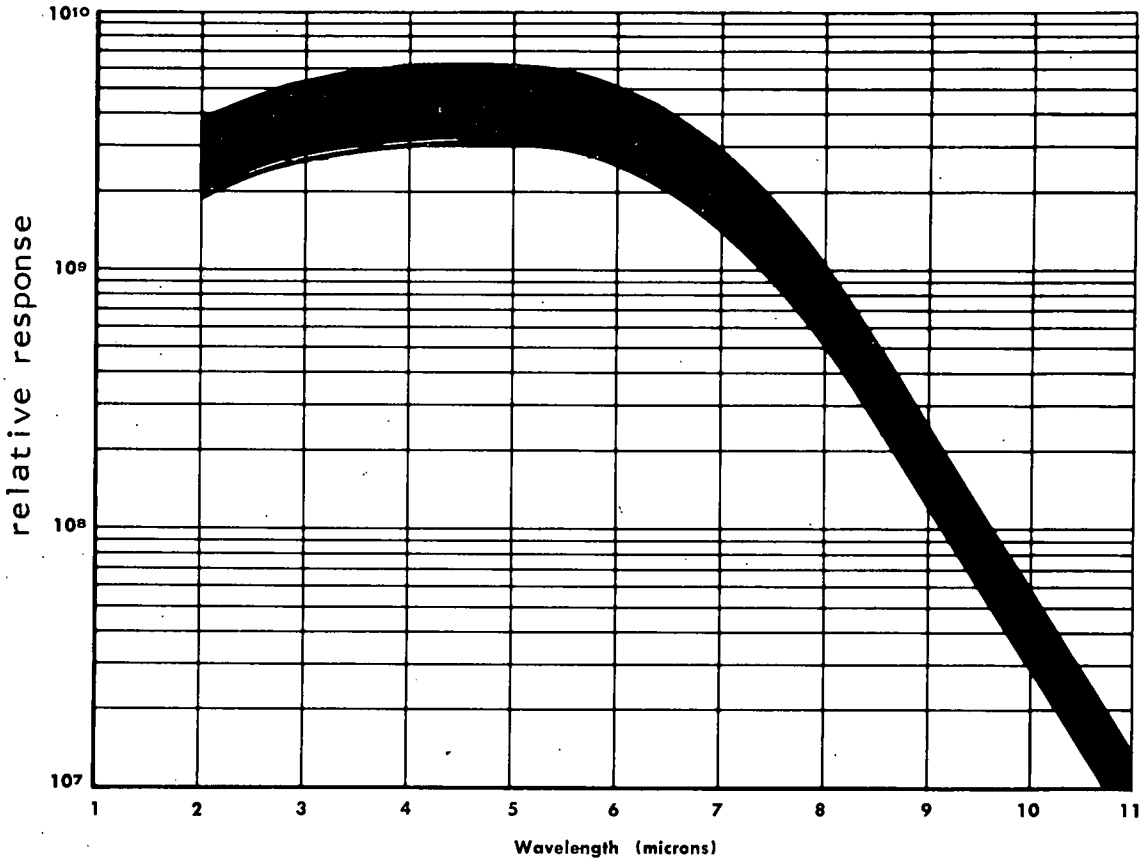

Figure 2.3 A curve of the relative response of the IR detector over its usable band. The peak responsivity at 4.5μm. is 2.4 mv/mw when operated from a bias of 75V into a load of 500Ω.

the detector had to be well shielded from noise. When the focus is formed, the large di/dt causes transients which generate r.f. noise. For example, a shorted co-axial cable would pick up $\sim$ 0.1 V of noise from these transients. The best shielding arrangement consisted of solid outer conductor co-axial cable using type N connectors. This cable was covered by solid copper tubing bolted to the screen room at one end and connected to the can on top of the detector dewar with eight layers of shielded braid. The can on the dewar houses the preamplifier for the detector.

With this arrangement, noise was typically $\sim$ 1 mV., but with tight shielding from the pipe to the can, it could be reduced to $<$ 100 μv.

With this noise shielding the minimum detectable signal was set by the level of hard x-ray pulse that could get through the x-ray shielding. This shielding consisted of a $1\frac{1}{2}$" thick cast lead cylinder open at one end. The detector had no direct view of the focus. The IR spectrograph and electrical noise shields also had to be shielded with $\sim$ 1.5 cm. of lead to prevent scattering of hard x-rays into the detector. Even with this shielding an occasional signal $\sim$ 10 mV. was detected due to x-rays. These "superbursts" also entered the neutron detector, so that these spurious signals on the IR output could be recognized and discounted. A general x-ray level of $\leq$ 3 mV. represented the minimum detectable signal.

2.3.2 SPECTRAL ANALYSIS

Spectral analysis of bremsstrahlung and scattered signals was done either with line filters of 10.6μ or 5.3μ (both have sideband suppression $\leq 10^{-3}$) or a salt prism spectrograph. The filters were used when possible due to their low loss as compared with the spectrograph. Approximate absolute power measurements were made using the 5.3μ filter and detector calibration specified by the manufacturer. Since the size of the focus is known at best to an order of magnitude, an exact calibration is meaningless. The 5.3μ filter gave sufficient transmission to allow operation of the detector into 50 Ω. With this arrangement the best time response was obtained limited by the bandwidth of the oscilloscope (Tektronix 556, BW = 50 mc.).

The spectrograph was a Perkin Elmer 12B. The salt prism of the spectrograph was slightly fogged making it necessary to block part of it off to prevent scattering. The slit was opened 2 mm. to allow imaging of the whole focus region into the spectrograph. As the focus moves stochastically ~ 1 mm. from shot to shot a 2 mm. slit together with a $\frac{1}{2}$ magnification of the optical system insured that the full focus plasma was viewed.

The bandwidth of the spectrograph had increased over the manufacturer's specifications due to masking the prism, imperfect spectrograph alignment and underfilling of the collimating mirror. The bandwidth at 10.6μ was measured using a CO_2 laser and was found to have increased by a factor of 2. This was assumed to be true across the spectrum. With this correction to the manufacturer's specifications the bandwidth had range from 2.4μ at

4μ to 1μ at 10μ for the 2 mm. slit. The exit slit was imaged onto the detector which is 2 mm. in diameter. Due to losses in the spectrograph the detector was operated into 500 Ω to maximize responsivity.

The IR detector has an intrinsic response of the Ge alone in addition to the extrinsic response of the impurity. This intrinsic response peaks at 1.5μ and has a responsivity 10 times that of the extrinsic region. In order to keep stray light at this wavelength from giving erroneous readings in the region beyond 7μ, a Ge window was placed over the entrance slit of the spectrograph.

2.3.3 OPTICAL SYSTEM

The optical system can be seen in figure 2-4. Mirrors were used primarily for cost reasons. The use of mirrors for off axis imaging implies astigmatism. However, this problem was not too important since only broad band measurements are needed to examine bremsstrahlung and scattered light. As can be seen in figure 2-4, the pickup mirror has a $\frac{1}{2}$" hole in it for the incident laser beam. The pickup mirror defines the solid angle of the receiving optics as $\Delta\Omega = 7.5 \times 10^{-3}$ steradians, with a receiving angle θ of 0.7° to 3°. The magnification of the system is $\frac{1}{2}$. The focal volume is $\Delta v = \ell\sigma$ where ℓ is the plasma length and σ is the imaged area of the detector ($\sigma = 2\pi$ mm.^{2}).

A NaCl window was used to close off the vacuum. Salt has a low dielectric constant from U.V. to 15μ ($\epsilon = 2.3$) and

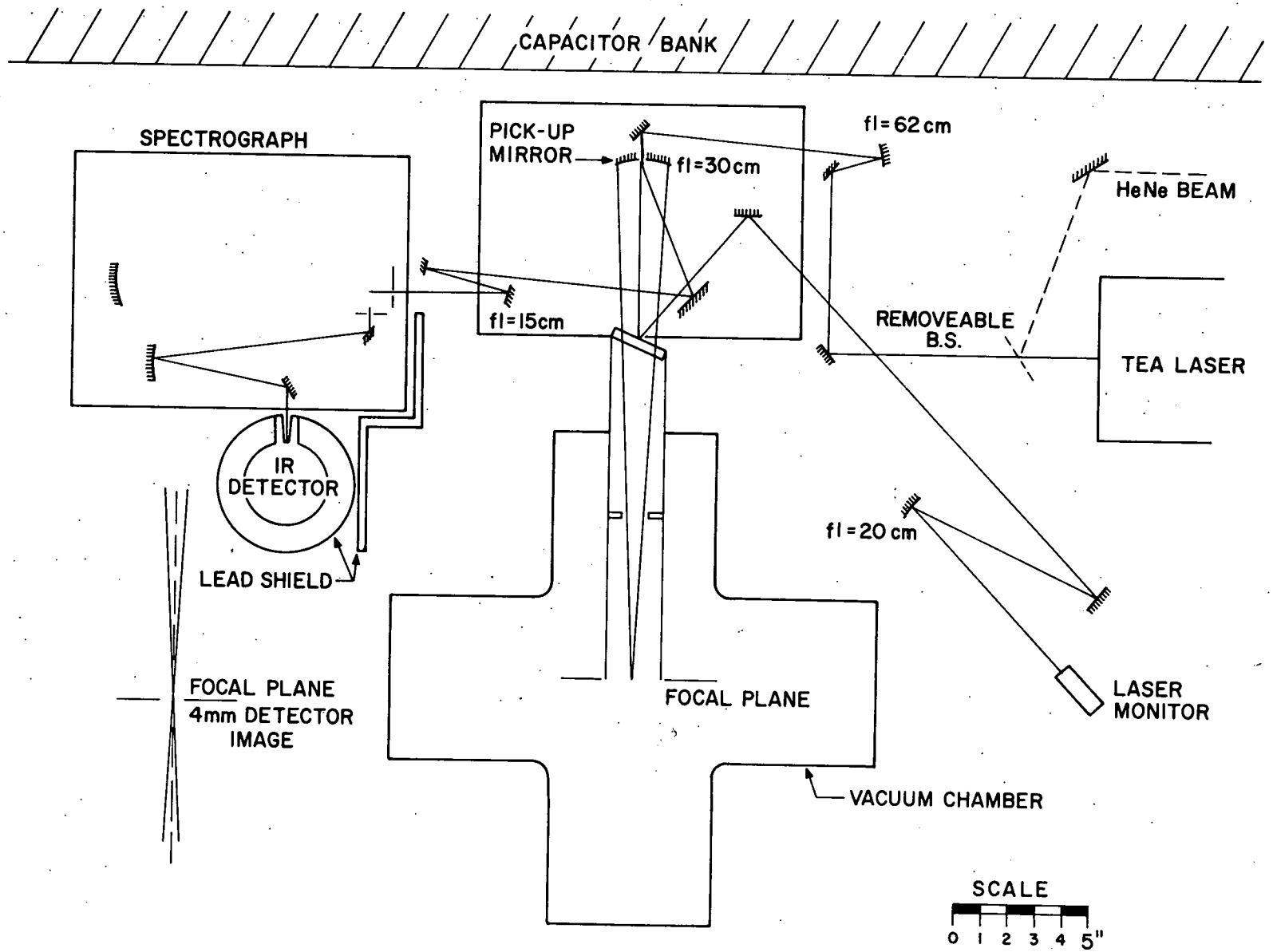

Figure 2.4 The layout of the optical system built around the plasma focus apparatus. The TEA laser and associated optics are on the right side while the detection system is on the left. The spectrograph may be removed and the detected light focussed directly into the detector for use with filters. The limiting rays of the detection system are shown on the left and are seen to be nearly paraxial.

therefore has low reflection loss. However, it has the disadvantage of etching along crystal planes from contact with the hot plasma. This necessitated regrinding the window surface after 50 shots, in addition to frequent cleaning to remove evaporated deposits. Irtran 2 (ZnS) was tried since, being an amorphous solid, it etched more uniformly. However, under the intense flux of x-rays, the window became lossy and could not be used.

Alignment of the optics was done with a movable jig which fit into the end of the hollow electrode. A $\frac{1}{4}$ in. diameter flat faced lamp, having a ground surface, could slide into the hole in the jig. The location of the lamp was at the center of the focus region. The light from this lamp could be followed through the optical system and focussed onto the entrance slit of the spectrograph or, when filters were used, directly onto the IR detector. With the spectrograph wavelength set in the visible red, the image could be followed through to the detector.

The focus plasma always remained in the field of view of the detection system as witnessed by low shot-to-shot variation ($\sim$ 20%) of the emitted light in the high frequency region (i.e. $\omega > 3\omega_{pe}$) between any two shots. Furthermore, when the axis of the optics was shifted to view the volume adjacent to the focus, the amplitude dropped by an order of magnitude. (This residual emission is caused by cool gas of the current sheet).

2.3.4 LASER

The laser used in these experiments was a transverse excited atmospheric (TEA) CO_2 laser. The discharge for excitation of the CO_2 takes place in a mixture of CO_2; H_e: N_2 at atmospheric pressure. In TEA lasers the fast discharge pumps the mixture in an interval short compared with the CO_2 relaxation time. As a result, gain switching is achieved[29] giving a giant pulse (duration ~ 150 nsec.) without the use of a Q-switch. The giant pulse is followed by a long tail ~ 300 nsec. of almost constant power equal to 10% of the giant pulse. The details of TEA lasers can be found in the literature[29]; the details of our laser can be found in the appendix. The power output ranged from 1 MW to 5 MW, depending on discharge current and gas mixture.

The laser beam was focussed onto the plasma focus region by a 62 cm. focal length mirror placed beyond the pickup mirror of the detection system. The spot size was 3 mm. x 4 mm., as measured by the burn pattern, and was limited by the laser beam divergence and physical restriction on the location of the focussing mirror. However, since the plasma focus does move somewhat, a large beam is desirable to insure full illumination of the plasma. With this arrangement the power level was ~ 10MW/cm^2. The incident power was monitored by focussing the reflected power for the salt vacuum window onto a photon drag detector.

Alignment of the laser focussing optics was made with a

HeNe laser beam. The HeNe beam was introduced into the CO_2 laser optical path by a "Handi Wrap" beam splitter. The red HeNe beam was made coincident with the 10.6μ beam by reflecting the red beam off the CO_2 laser output mirror and back onto itself. The CO_2 laser was then fired with the beam-splitter in place ("Handi Wrap" is 50% transmitting at 10.6μ) and the relative positions of the red and CO_2 beams could be compared by placing an oxidized piece of metal in the beam path.

The CO_2 laser beam alignment mirrors could be adjusted to focus the red beam onto a light target at the location of the plasma focus. The reflected red beam from the light target was imaged onto the detector with the spectrograph tuned to 0.6μ. Final adjustment was made with the CO_2 laser fired at the glass light target. As glass is a black body for 10.6μ only a small fraction of the incident beam was reflected.

By observing this reflected signal, the final adjustment of the incident beam location was made. Alignment had to be checked from time to time due to the large vibrations the mirrors received as a result of each discharge.

The beam dump was originally a metal plate which deflected the beam into the glass walls of the vacuum vessel. The residual backscattered signal from the chamber was on the order of a few millivolts. Since the current sheet is lossy, this residual would be absorbed. To check the dump arrangement, a ground salt diffuser was placed at the focal point in an attempt to simulate the refractivity of the plasma; no signal was picked up.

Yet during the course of the experiments large signals were observed at the incident laser beam frequency. As they had the proper time relation to the plasma focus, they were thought to be scattered signals. They were suspicious, however, since there was little correlation with the amplitude of the incident signal.

As a check, the alignment jig and beam deflector were replaced with an all-glass beam dump and the large signals mentioned above disappeared. The remainder of the scattering experiments were done with this beam dump.

3. PRESENTATION OF DATA

In this chapter we will present and briefly describe data obtained in the focus experiments. Most of the data presented was taken with the hollow anode (center electrode), but some data of streak and framing photographs was taken with a solid electrode run at negative potential. The qualitative features of this data are still the same as those for the hollow anode and are shown as visible light photographs to provide a physical understanding of the size, shape, etc. of the plasma flow. As di/dt wave forms are also different for solid vs. hollow center electrodes, timing measurements made relative to this signal can only be compared qualitatively.

3.1 TERMINAL CHARACTERISTICS

The current i, di/dt and V, the voltage across the breach of the co-axial accelerator, are shown in figure 3-1 on a slow time scale. This data was taken with a hollow center electrode run as an anode. The filling pressure was 1.6 torr D_2 + 3 % Ar; operation at lower pressure (1.1 torr D_2 + 5 % Ar) gave substantially the same wave forms. Note the large spike in di/dt and V due to the $i\frac{dL}{dt}$ of the collapsing current sheet. The current falls slightly due to work done during collapse and the increased circuit inductance associated with the pinch filament ($\sim$ 15nH). For a bank voltage of V_B = 32 kV the current (I_p.) just following the peak in di/dt is 320 KA.

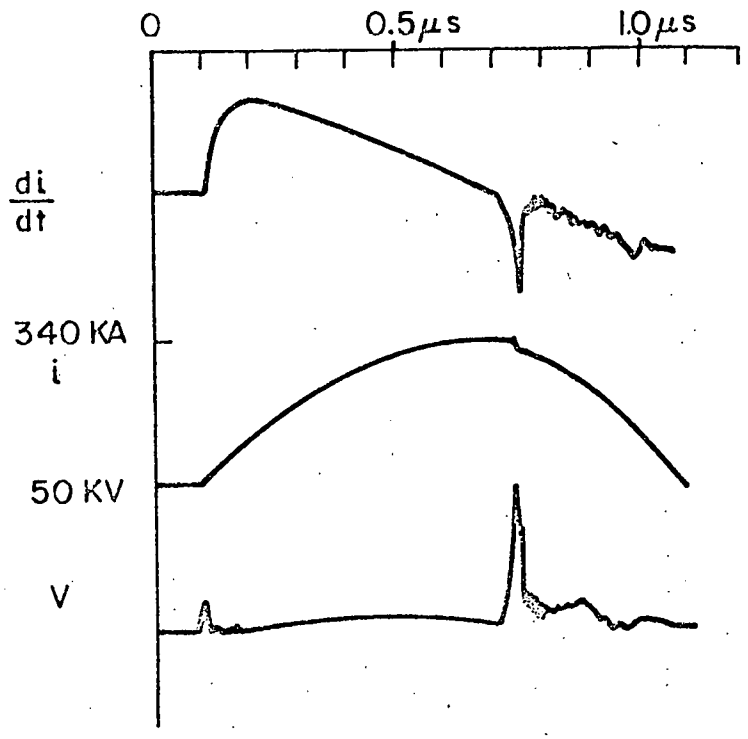

Figure 3.1 Waveforms of di/dt, i, v (measured across the breach of the co-axial accelerator). The fall in di/dt at current maximum corresponds to the formation of the plasma focus.

3.2 VISIBLE LIGHT PHOTOGRAPHS

During the spike in di/dt, the visible light shows the collapsing current sheet (fig. 3-2). This set of three photographs, taken with a solid electrode, shows (A) the collapsing current sheet early in the rise of di/dt. Fifty nanoseconds later (B), one sees the pinch form and then 50 ns. later (C), the luminosity has decreased markedly and the region of visible light on the axis appears to have diffused.

The decrease in luminosity can be seen as a continuous function of time in a streak photograph. Figure 3-3 shows a streak taken 1 cm off the center electrode. One sees a luminous sheet moving towards the axis with a velocity of 25 cm/μsec. As the current sheet converges into the axis, there is a transient increase in luminosity which occurs near the peak in di/dt. This transient increase lasts for a few tens of nanoseconds and is followed by an abrupt decrease in luminosity. For ionizing shock speeds of 25 cm/μs. in H_2 the post-shock temperature $(T_e + T_i)$ is $\sim$ 60 eV. As a result, the plasma is fully ionized and the luminosity has been interpreted as free-free bremsstrahlung.[6,19] After the pinch forms on axis, the temperature and density should go still higher due to magnetic compression so that one is left trying to guess the reason for the decrease in luminosity.

The bright region on the right of fig. 3-3 is caused by metal vapor from the center electrode and occurs well after the neutron emission. The vertically moving pairs of lines occur towards the end of neutron emission; their origin is uncertain.

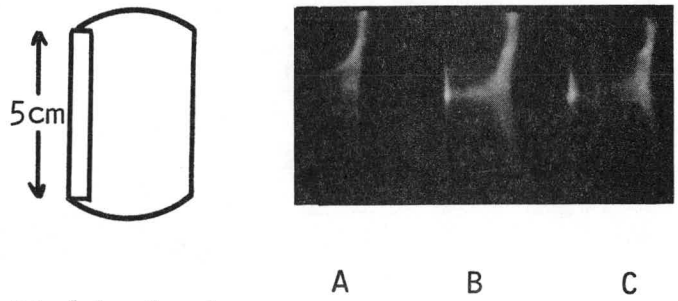

Figure 3-2

Three framing photographs (10 nec. exposure) take 50 nsec. apart; pressure is 1.6 torr of H_2 with I_p = 270 KA. taken with solid center conductor. A take during collapse, B at formation of pinch, C,50 nsec.later. Figure at left shows field of view off end of center conductor.

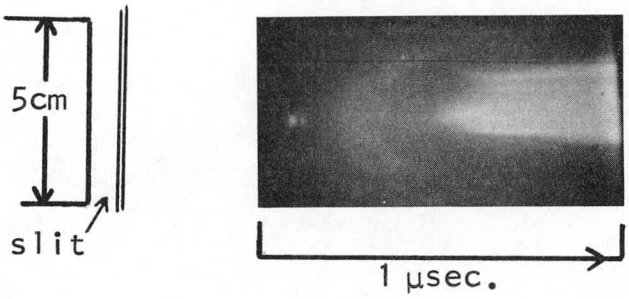

Figure 3-3

Streak photograph of 1 μsec. duration taken 1 cm. of solid center conductor. Pressure 2.16 torr H_2 with I_p = 270 KA.

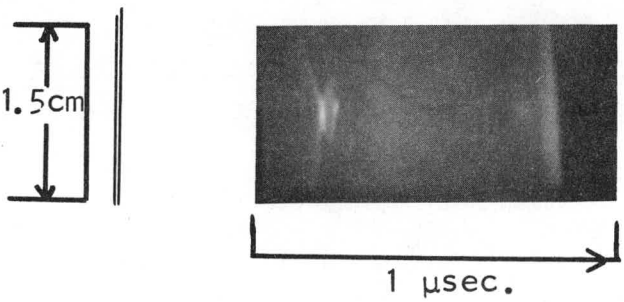

Figure 3-4

Enlarged streak photograph taken at 2 torr H_2 + 5% Ar at I_p = 270 KA.

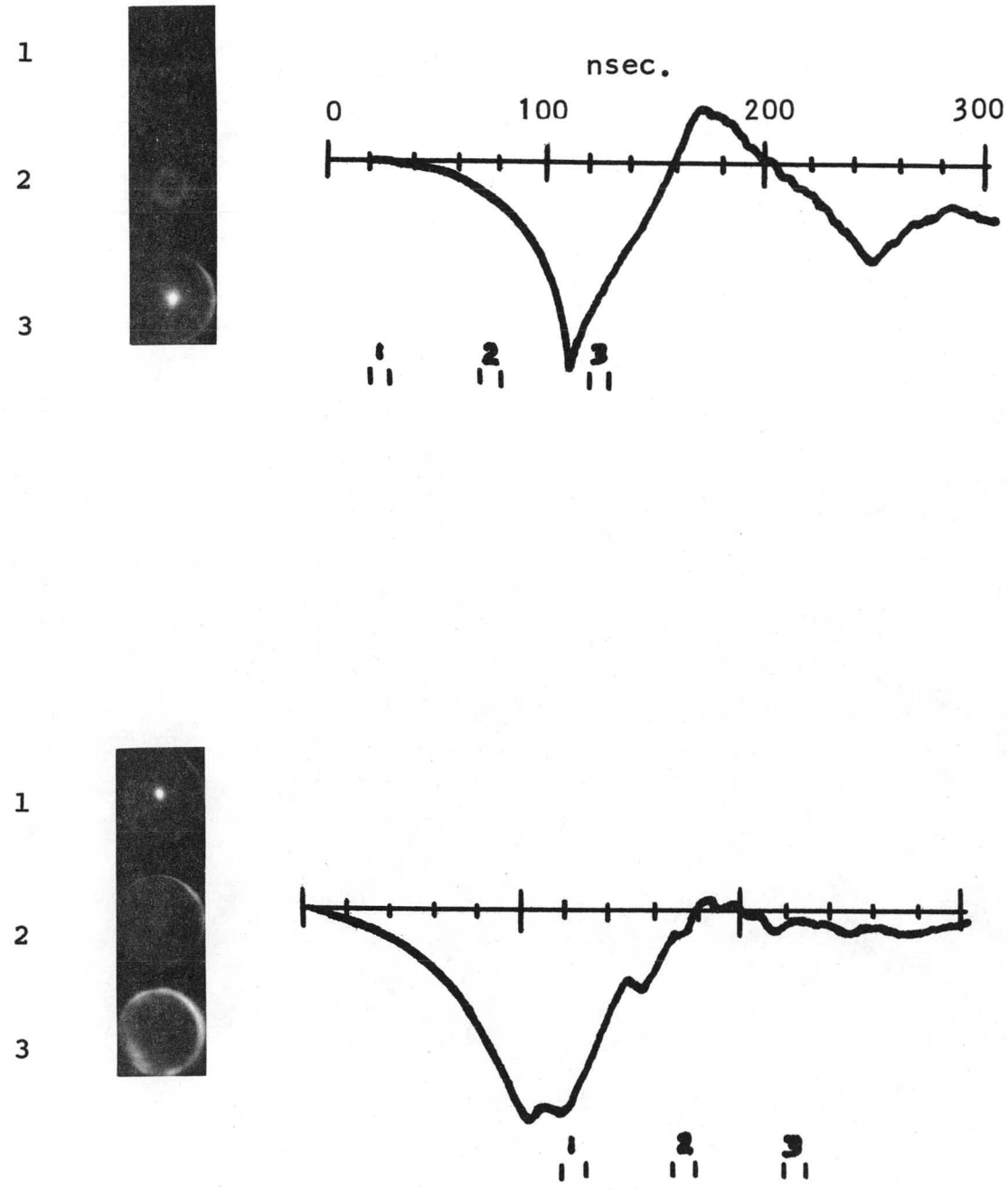

Figure 3-5

Framing photographs (10 ns exposure) take axially 50 nec. apart using hollow anode. The pressure is 2.3 torr H_2 + 10% Ar. with I_p = 310 KA. Traces on right give timing of photographs relative to di/dt.

Figure 3-4 shows a streak photograph taken with a times 3.3 magnification over fig.3-3. The plasma column diameter before the decrease in luminosity is ~ 1mm.

Figure 3-5 shows framing photographs taken up the axis of the hollow anode. The argon concentration is 10%, somewhat higher than in the rest of the work. (The additional argon keeps the focus visible for a longer period of time). The light now is integrated along the axial direction, thereby increasing the contrast of the light of axially aligned plasma relative to return current sheet. As a result, the current sheet is not visible in the photographs. The bright region is ~ 3 mm. in diameter and occurs near the peak in di/dt.

3.3 X-RAYS AND NEUTRONS

Figure 3-6 shows a composite of hard x-rays, neutrons and soft x-rays with di/dt as a reference. The hollow anode was used; filling pressure was 1.2 torr D_2 + 4% Ar with I_p= 320 KA. The traces are taken from three different runs with 2 soft x-ray emissions displayed to give an indication of shot-to-shot variation. With the hollow anode, metal vapor flows into the plasma after 500 ns. so that the x-ray radiation shown is solely from the D_2+Ar plasma. One should note that soft x-rays are still emitted by the plasma well after the dense pinch phase, the end of visible radiation and neutron emission. The delay of the start of the hard x-rays relative to the soft x-rays is typically 40 ns.; however, the hard x-rays show wide variation in timing (+20,-40 ns.), size and duration.

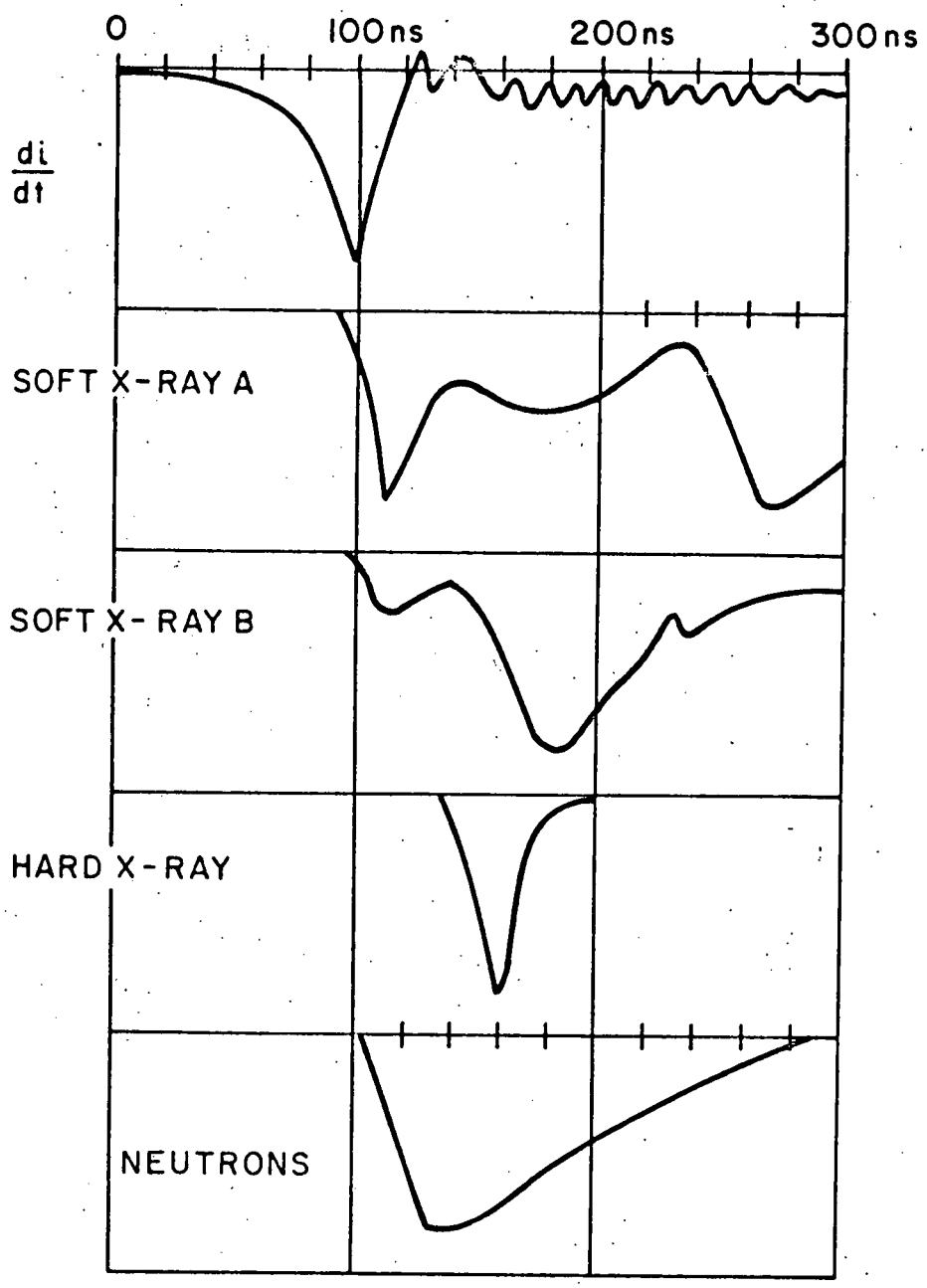

Figure 3.6 A composite di/dt, soft x-rays, hard x-rays and neutrons taken from several shots at I_p = 320 KA. in 1.2 torr D_2 + 4% Ar. Two soft x-rays (A and B) are shown indicating typical variation. Maximum timing error ± 15 nsec.

A typical neutron pulse (time of flight corrected for 2.45 MeV) shows a half width of ~ 100 ns. The range of total neutron emission is 10^8 to 10^9 and is typically 8×10^8, as measured by a silver foil activation technique.

3.4 INFRARED BREMSSTRAHLUNG

The first bremsstrahlung measurements were made using the salt prism spectrograph and an IR detector rise time of $T_r \cong 30$ ns. The focus was operated with a filling pressure of 1.6 torr D_2 + 3 % Ar and a pinch current of 320 KA. A composite of bremsstrahlung data taken at 2μ, 5μ, and 6.7μ, with their relationship to di/dt and neutrons, is shown in figure 3-7. The 2μ data shows the normal IR emission which was interpreted as free-free bremsstrahlung with no nonthermal effects. The thermal bremsstrahlung starts with the neutron emission but always decays faster; it subsequently decreases to ~ 10 % of its peak value and remains constant until, after 500 ns., wall impurities enter the plasma. This persistent radiation is due to emission from both the return current sheet and the plasma left after the dense pinch has broken up. In addition, the level of the persistent radiation sets an upper limit to the contribution from the cool gas of the return current sheet.

Emission at 5μ ± 1.1μ is given as 2 typical curves. The one referred to as thermal has the same shape as the 2μ emission and is most frequently observed. One shot out of ten taken in this series of measurements showed an enhancement which turned on abruptly at about the time the dense pinch phase ended. The

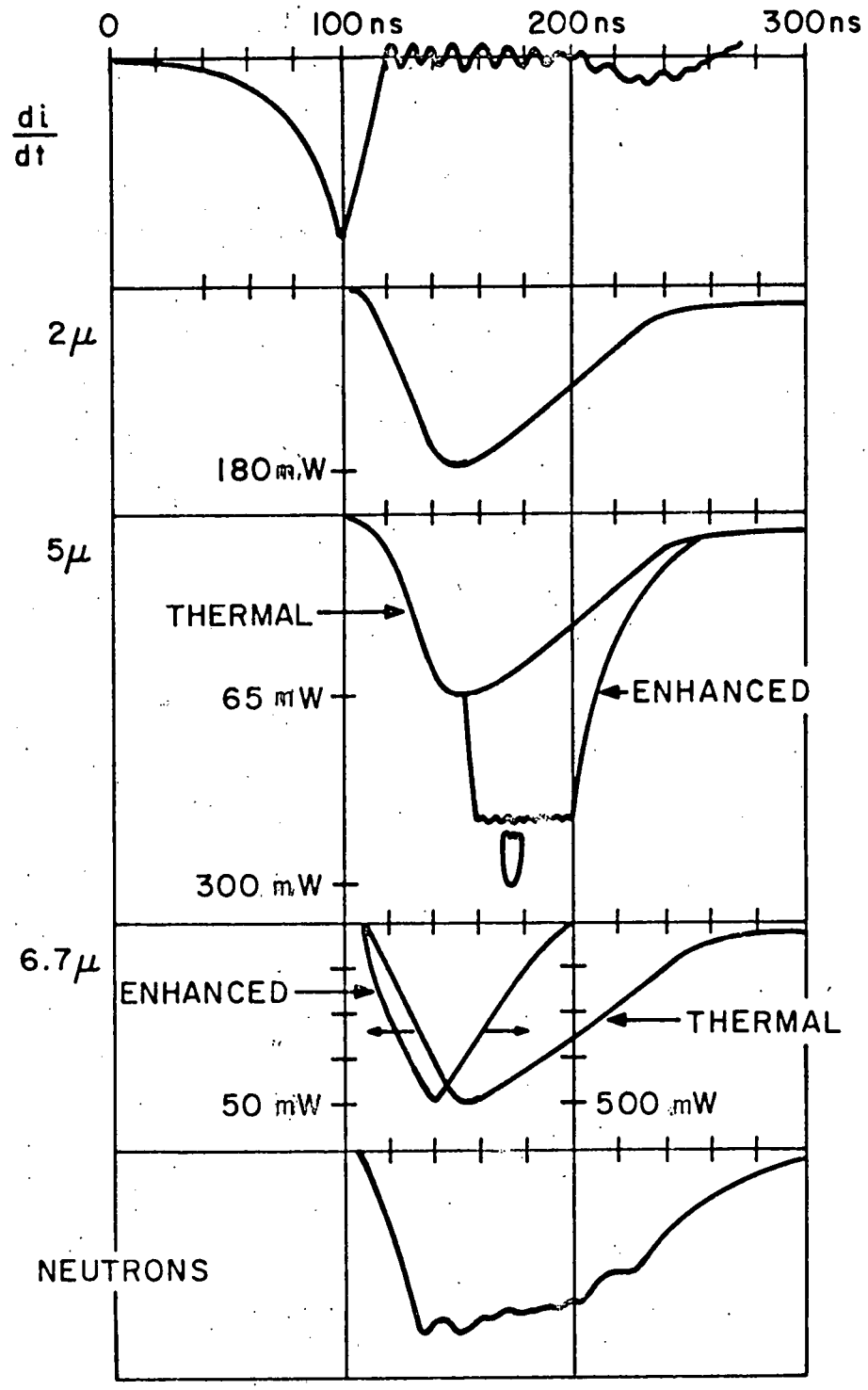

Figure 3.7 Composite of di/dt, thermal and nonthermal bremsstrahlung and neutrons taken at 1.6 torr D_2 + 3% Ar., I_p = 320 KA. Detector rise time 30 nsec., maximum relative timing error is ± 15 nsec.

enhancement here is ~ 5 over thermal. At 6.7μ ± 0.7μ two curves are also shown, one being the more frequent thermal emission and the other enhanced, this time, 10 times thermal. In contrast to the enhanced emission seen at 5μ, at 6.7μ (and also 8.5μ--not shown) the super thermal emission begins with no measurable delay relative to thermal emission. This emission lasts on the order of the duration of the dense pinch phase and then decays down to thermal levels. Enhancement at longer wave lengths had a maximum of 100 times thermal.

In figure 3-8 is plotted the peak value reached by the IR emission in a scan taken from 2 to 10.6μ, under the same conditions as the data in fig. 3-7. The resultant large scatter of the data is a characteristic of plasma focus measurements, together with the added problem of film deposits on the window. The absorption from these deposits is known only to within ~ 25 per cent. The data has been corrected for detector responsivity, spectrograph bandwidth and absorption, as well as window loss.

The data in fig. 3-8 is sufficiently accurate to reveal the essential features: (1) that from 2 to 6μ the received power falls off as $1/\lambda^2$, as is expected for thermal bremsstrahlung, and the received power is the correct order of magnitude for a thermal plasma of $n = 3 \times 10^{18}/\ cm^3$, T_e = 750 eV, with a volume of $3 \times 10^{-2}\ cm^3$; and (2) that enhanced emission occurs during the whole duration of the dense pinch phase for $6.5\mu < \lambda < 9\mu$. Enhanced emission may also have occurred for wave length $\lambda > 9\mu$ but would not have been observable due to decreasing sensitivity

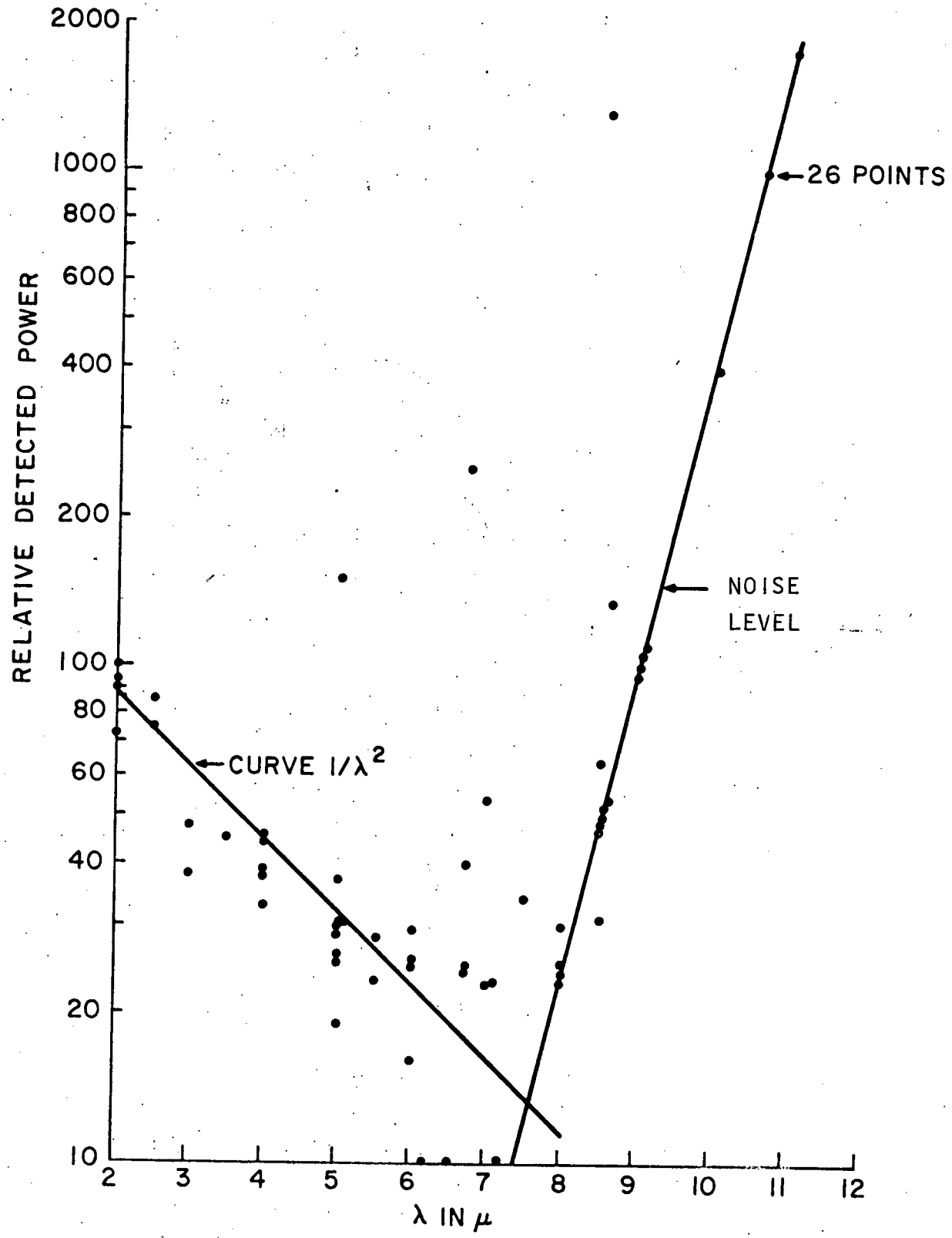

Figure 3.8 Graph of relative power received from plasma focus. Data is a composite from many runs at 1.6 torr D_2 + 3% Ar., I_p = 320 KA.

of the IR detector. Note that all data above noise level for $\lambda > 6.5\mu$ shows some enhancement. Observation of large enhancements was infrequent -- in the range $6.5\mu > \lambda > 9\mu$ only 3 observations out of 26 showed enhancement greater than 10 times thermal.

Figure 3-9 shows more data taken at p = 1.6 torr D_2 + 3% Ar and I_p = 320 KA. This data was obtained using the same optical system, but the spectrograph was removed, and line filters were substituted. This system gave less light loss so that the IR detector could be operated directly into 50Ω, which resulted in an electrical bandwidth limited by the oscilloscope ($T_R \sim 7$ nsec.). The 5.3μ filter has a bandwidth of 0.5μ full width at half maximum (FWHM). Shown also relative to di/dt are neutrons and visible light (0.4μ to 0.7μ). The visible light electrical bandwidth is also limited by the oscilloscope ($t_R \sim 7$ nsec.). The IR emission has a rise time ≤ 7 nsec. (correct for scope rise time) and a duration at peak intensity equal to that of the dense pinch phase of the plasma focus. The IR emission then shows a slow decay over 60 nsec. to the residual level of ~ 10% of the peak.*

---

* With this optical system, losses are easier to take into account, allowing us to compare the received power to that emitted by a thermal plasma. As seen in figure 3-9, the power received at 5.3μ is 45 mw or 12 watts/str. μm, with a correction made for the filter loss, but not including a window loss of ~½. A plasma with a volume of 3×10^{-2} cm³ with T_e = 750 eV and density $n_e = 3 \times 10^{18}/cm^3$ taking into account 3% Ar stripped[4] to Z ~ 10 emits free-free bremsstrahlung as[45]

$$j\omega = 5 \times 10^{-52} \frac{n_e}{T_e^{\frac{1}{2}}} \sum_i n_i Z_i^2 \quad \text{watts/m}^3 \text{ str. rad/sec.}$$

which yields an emitted power of 53 watts/str. μm. The plasma

Once again there is an enhanced emission at the end of the bremsstrahlung emission from the dense pinch phase, although with faster time response its true duration is seen to be < 20 nsec. Comparing the neutron and IR emission, the duration of neutron emission is about twice that of the IR emission.

Visible light is also shown and should be compared with the IR emission. The visible light was observed using the same optical system used for the IR measurements in order to achieve an identical field of view. The data is from different shots, but it was taken on the same run with identical conditions (bank energy, gas pressure, etc.). The data was taken over a number of shots to be sure of temporal reproducibility which was found to be within the resolution of the instruments (± 15 nsec.). One sees clearly that visible and IR emission do not have the same amplitude variation which casts some doubt on the interpretation of the visible emission as dominated by free-free bremsstrahlung.**

---

parameters used are calculated in chapter 4 and are at best correct to within a factor of 2 so that under these conditions the agreement is good.

** It should be pointed out that in experiments[8, 19] where streak photographs have been interpreted in terms of free-free bremsstrahlung, the measured shock speeds were ~50 cm./μs or 2 times greater than ours, which implies a post-shock temperature 4 times higher. Under this condition the assumption of free-free bremsstrahlung is more justified since T_e is then on the order of ten times the ionization energy. Even so, our streak photographs show the same luminosity variation as those of Toepfer. Moreover, Potter's code gives postshock temperature, substantially lower than plane shock theory predicts. The lower electron temperature given by Potter precludes interpreting the light as free-free bremsstrahlung.

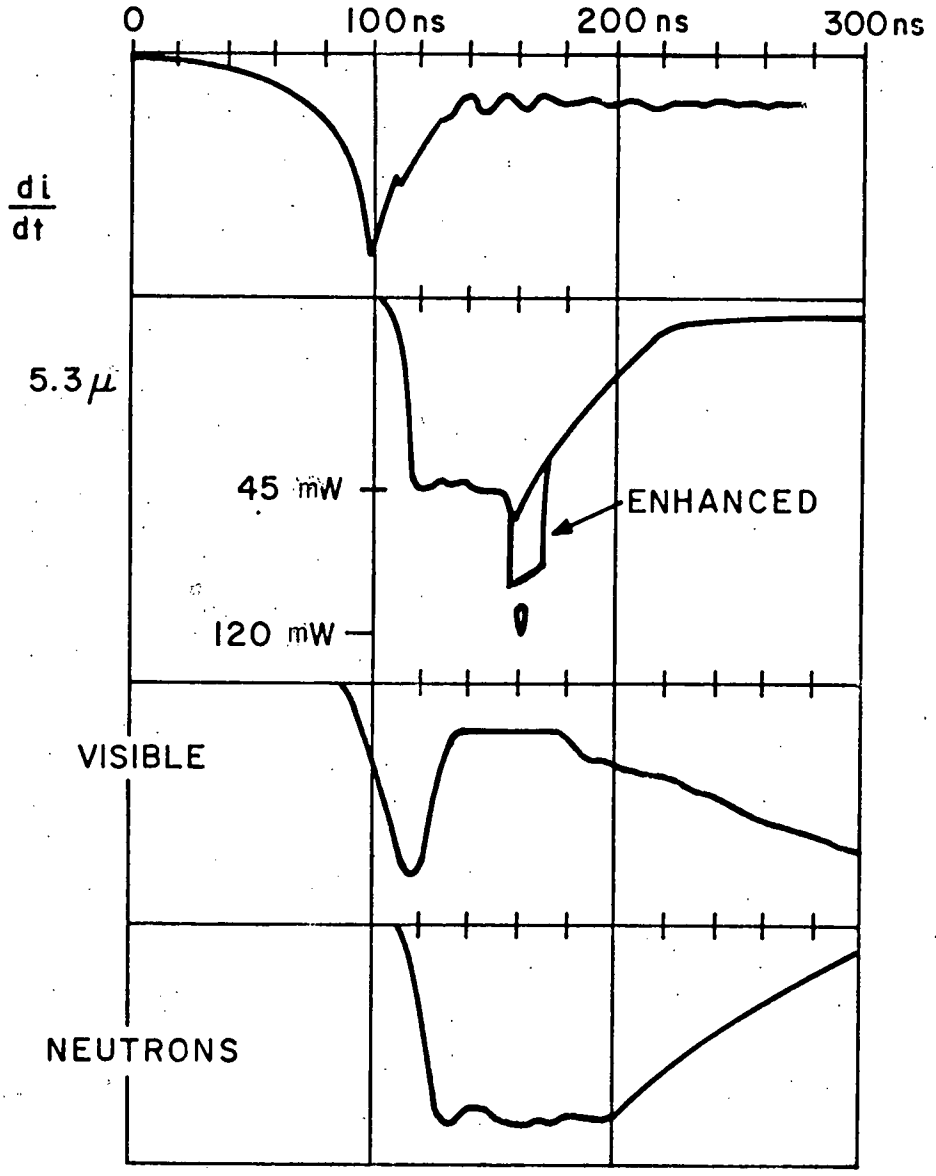

Figure 3.9 Composite of di/dt, 5.3 μ emission, visible (0.5μm), and neutrons taken from different shots at 1.6 torr D_2 + 3% Ar. I_p = 320 KA. Instrument rise time 7 nsec. for the IR and visible data, the maximum timing error ± 15 nsec.

Figure 3-10 presents the most striking data. The focus was operated at p = 1.1 torr of D_2 + 5% Ar with I_p = 320 KA. A 10.6μ, 0.28μ FWHM line filter was used in place of the spectrograph. The peak IR emission measured was 4×10^6 over thermal bremsstrahlung. The duration and intensity variation relative to the thermal emission at 5.3μ are distinctly different from the nonthermal emission observed at higher pressures(1.6 torr). One should note that peak emission comes during and after the drop in density. Emission at 10.6μ corresponds to frequencies $\sim 4(\overline{\omega_{pe}})_{max.}$ or $25\ \omega_{ce}$. Measurements with the spectrograph at other wavelengths for this operating condition showed one enhanced emission at 7μ starting 100 nsec.after the peak in di/dt. The probability is much better for seeing enhanced emission at 1.1 torr pressure. Out of 20 measurements at 10.6μ, 9 showed enhanced emission.

In addition to these measurements at filling pressure of 1.6 torr and 1.1 torr, measurements were made at 0.9 torr to check the pressure dependence of 10.6μ radiation. Of 25 measurements, only 2 showed enhanced radiation at this wavelength (see table 3-1). At this pressure the maximum radiation level received was 5 watts, with a full duration of 200 nsec. starting with the fall of di/dt, characteristic of the 1.1 torr data.

TABLE 3-1 EMISSION AT 10.6 μm.

PRESSURE IN TORR	0.9	1.1	1.6
NUMBER OF MEASUREMENTS	25	20	26
NO. OF EMISSIONS > 10 THERMAL	2	9	0

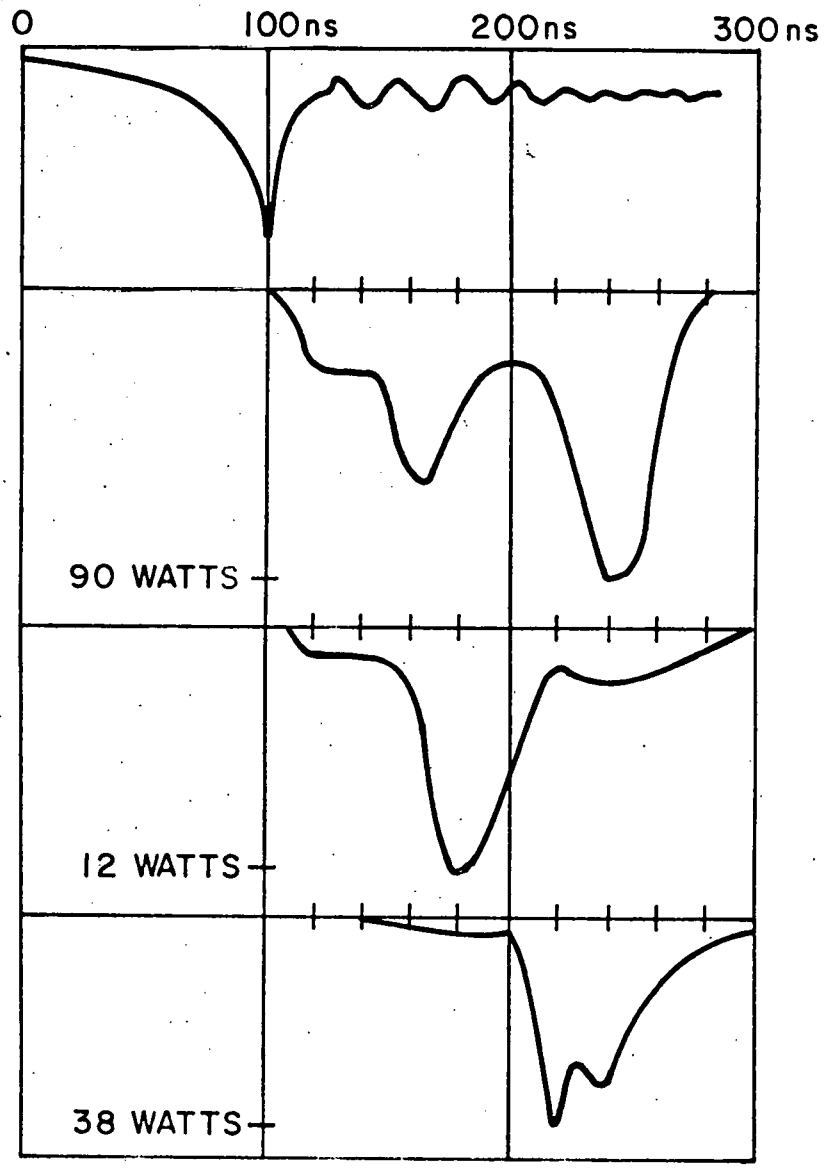

Figure 3.10 Nonthermal emission at 10,6μ, 0.28μ FWHM taken with I_p = 320 KA at 1.1 torr D_2 + 5% Ar.

3.5 LASER MEASUREMENTS

An attempt to scatter from electron fluctuations was made while operating at 1.6 torr D_2 + 3% Ar. Initial measurements showed no enhanced scattering in the band 5μ to 9μ. In runs made shortly after these, enhanced bremsstrahlung was observed and interpreted as $2\omega_{pe}$ emission. Since this band is the same as the band for scattering from ω_{pe} fluctuations, further work was abandoned, because it would have been impossible to distinguish between scattering and the enhanced emission.

Our efforts concentrated on scattering from low frequency fluctuation ($\Delta\omega \sim 0$). Using the all-glass beam dump, we observed no scattered signals of satisfactory amplitude over background noise.

Many backscattered signals were observed with the first beam dump. However, these are now understood to have been caused by laser radiation refracted by the plasma onto part of the beam dump, which then reflected a fraction of the radiation back into the detector. A typical observed signal reflected from the dump is shown in figure 3-11. The angular deviation of this refracted signal is $\leq 6^\circ$ from the forward direction. The signal was refracted from the tail of the laser pulse where the amplitude was constant at 100 kw. Although the scattering cross section could not be determined due to the way the measurement was made, it is clear from the magnitude of the received power that single-particle scattering was not responsible and that the

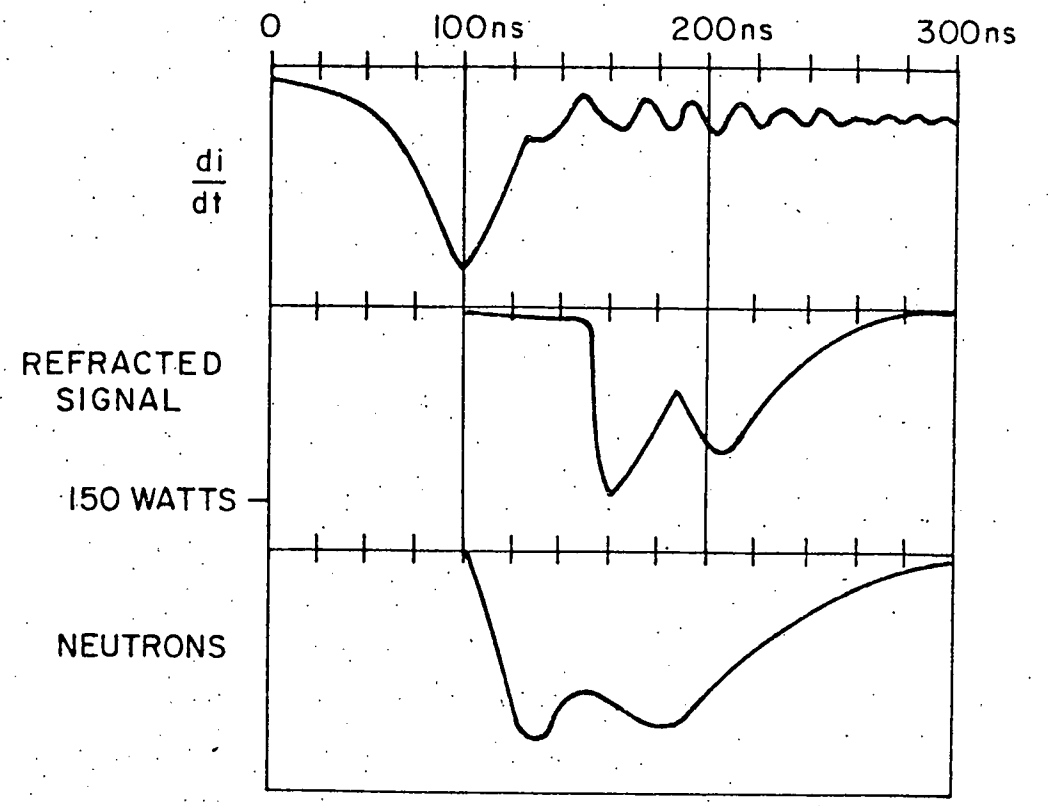

Figure 3.11 The refracted signal which appears at the end of the dense pinch phase shown relative to di/dt and neutrons.

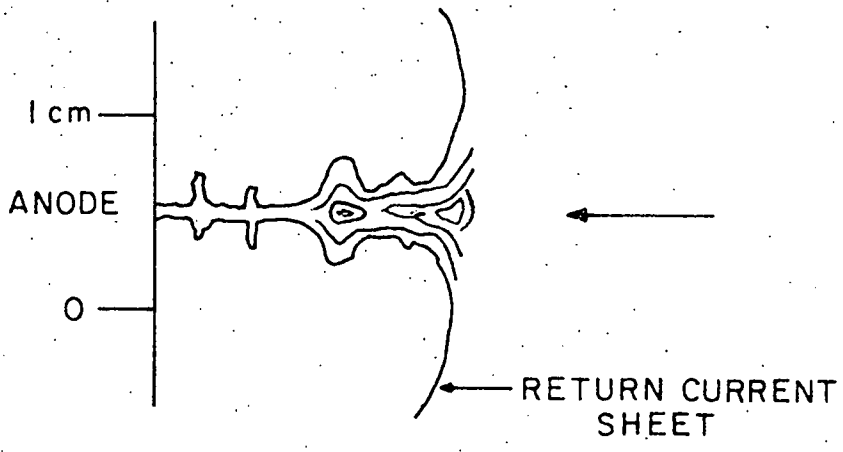

Figure 3.12 Outline of density contour reproduced from Peacock's interferogram, showing refractive plasma at end of the pinch.

total beam was deviated through a small angle.

This data was taken from a run at 0.9 torr D_2 + 5% Ar at I_p = 320 KA. During one run with the laser, every shot (out of 12) yielded a signal similar in form to that shown in figure 3-11, whereas nonthermal radiation was emitted in only 2 shots out of 25 (laser off). The detector rise time was 30 nsec. in this measurement so that the amplitude of the peak was larger than that shown in figure 3-11.

3.6 DISCUSSION OF LASER MEASUREMENTS

Two types of scattering are possible when the signal to be detected is near the transmitter wavelength ($\Delta\lambda/\lambda \sim 3 \times 10^{-2}$): coherent scattering (reflection) from a critical surface ($\omega_i = \omega_{pe}$) and incoherent scattering from underdense plasma ($\omega_i > \omega_{pe}$). Coherent scattering takes place during the dense pinch phase or possibly during and following the pinch break-up, particularly if local regions of high density persist in a generally underdense plasma. Incoherent scattering could occur near the central line only in the low density plasma remaining after pinch breaks up, since during the pinch $S(k,\omega)$ (for $\omega < \omega_{pi}$ and $k \sim \frac{1}{2}\lambda_D$) has been observed to be within a factor of 3 of $S(k,\omega)$ for a thermal plasma[31] (see chapter 4 for discussion). However, we observed no scattering of either kind. The following discussion attempts to explain this, as well as to understand the refracted signal of figure 3-11.

3.6.1 REFLECTION

When the laser experiments were begun, no interferograms of the focus were available. It was inferred[1,5] from neutron emission that pinch densities should be from $10^{19}/cm^3$ to $10^{20}/cm^3$. As was pointed out in the recent analysis[32], Peacock's interferograms show that a region of $n_e > 10^{19}/cm^3$ exists only on axis with a radius of 200μ and length of 5 mm. (resolution ~ 100μ). In our experiment the magnetic pressure is ~ $\frac{1}{4}$ of that of Peacock's experiments, implying that the overdense region is even smaller if it exists at all.

Ignoring refractive loss for the moment, the minimum size of a totally reflecting object (assumed to be spherical) which can be detected can be found from geometrical optics. For all but the forward direction, $\frac{dP_s}{d\Omega} = I_i \frac{\sigma_s}{4\pi}$, where P_s is the scattered power and I_i is the incident power per unit area. Taking the minimum for P_s as ~ 1 watt and $I_i = 10^7 w/cm^2$ gives $\frac{\sigma_s}{4\pi} = \frac{I_i}{\Delta\Omega} \Rightarrow$ a radius $a \cong 100\mu$.

Refractive loss will increase the minimum detectable size. The interferogram shows that the accessibility of the dense pinch is not good. Figure 3-12 shows an outline of the density contour reproduced from the interferogram. From the view of the dense pinch indicated by the arrow there exists a volume of intervening plasma with length $\ell \leq 1$ cm. and radius $r_o \sim 2$ mm. We assume that with the hollow electrode an equivalent volume exists at the opposite end of the pinch. The peak density is ~ $5 \times 10^{18}/cm^3$ (Peacock's experiment) and, although absorption is not strong (since T_e is high), refraction will deflect the

incident beam away from the dense pinch column effectively reducing its size (plasma acts as a negative lens).

To estimate the refractive effect, we consider a cigar-shaped plasma having a density profile $n = n_o e^{-r^2/r_o^2} \; e^{-z^2/\ell^2}$ where r_o and ℓ are the characteristic radius and length, and n_o the maximum density. The incident beam follows the ray equation[33] $\frac{d\varphi}{dz} = \frac{1}{\mu} \frac{\partial \mu}{\partial r}$ where μ is the refractive index ($\mu^2 = 1 - n/n_c$). We require that $\Delta\varphi$, the total change in φ from the incident ray direction, be small since the ray must remain almost paraxial in order to backscatter. We can therefore integrate along a straight line. We estimate refractive loss in this region by calculating the maximum impact parameter r for a ray to penetrate this region to the dense pinch. Under these conditions, with $n_o = 2 \times 10^{18}/cm^3$.

$$\Delta\varphi \sim 2\sqrt{\pi} \; \frac{n_o}{n_c} \; \frac{r\ell}{r_o^2} \; e^{-r^2/r_o^2}$$

We require $\Delta\varphi \lesssim 0.02 = 1.5°$ (half angle of detection system) and gives $r \lesssim 10^{-2} \, r_o$. As r_o, the pinch radius, is approximately equal to the beam radius, we find $\sim 10^{-4}$ of the incident beam intensity enters the dense pinch, reducing its apparent size by the same factor. This refractive loss prevents performing either coherent or incoherent scattering measurements during the dense pinch with the present system.

As will be indicated in chapter 4, there is also reason to believe that overdense regions may persist after the dense pinch phase in plasma where the average density is such that

$\omega_i >> \omega_{pe}$. In this case the refractive loss is much less than that indicated above for the dense pinch and a few hundred microns represents the upper limit to radius of an overdense clump of plasma persisting after the dense pinch.

3.6.2 REFRACTED SIGNAL

After the pinch phase, the density drops. This is seen in Peacock's interferograms[11] which indicate $n_e < 10^{18}/cm^3$, and also from the expanded plasma volume seen in C of figure 3-2. As seen in figure 3-11, the transparency increases abruptly, and continues for the duration of the neutron yield. Physically, one might expect macroscopic turbulence at this stage. However, the observed deflection ($\Delta\varphi \sim 0.1$) of the laser beam by the plasma may be accounted for either by a plasma having $n_o = 2 - 10^{17} cm^3$ and a cigar-shaped density gradient, or from random eddies of size $\sim 100\mu$ with $\frac{\delta n}{n} \sim 10\%$ (typical of Zeta turbulent fluctuation[34]). In the first case, we take $n = n_o e^{-r^2/r_o^2} e^{-z^2/\ell^2}$ with $\frac{n_o}{n_c} = 5 \times 10^{-2}$ and $\mu \sim 1$. Then

$$\frac{\partial\varphi}{\partial z} \sim \frac{\partial\mu}{\partial r} \qquad \Delta\varphi \sim 4\sqrt{\pi}\,\frac{n}{n_o}\,\frac{r\ell}{r_o^2}\; e^{-r^2/r_o^2}$$

In the expended plasma, $r_o \sim \frac{1}{2}$ cm. and $\ell \sim 2$ cm. yield $\Delta\varphi \sim 0.1$ for $r = 1$ mm. (the latter is characteristic of the laser beam size). On the other hand, deflection in a plasma having a large density fluctuation of $\frac{\delta n}{n} = 0.1$ but $\frac{\bar{n}}{n_c} << 1$ can be described by a linearized ray equation provided the laser wavelength is much smaller than the eddy size (no diffraction). Then quantity $\frac{\delta n}{\bar{n} - n_c}$ and

$\bar{n} - n_c$ are the only parameters which determine the φ rms = $\langle \varphi^2 \rangle^{\frac{1}{2}}$ on scattering from an eddy[34] (large eddies produce deflections due to the long length of the refracting path, but small eddies produce the same deflection due to their steeper gradient). For these parameters, the total number of eddies is ~ 200 and[34] φ rms. $= 10^{-2}$, then $\Delta\varphi \cong 0.14$. The refraction from eddies should add to the refraction due to gradients which leaves $\Delta\varphi$ the same; hence both are possible. Due to the imprecision of the measurement, little more can be said. What figure 3-11 does show, however, is that there is significant interaction between the plasma and laser beam, that the plasma transparency turns on very abruptly, and the refractivity lasts the duration of the neutron production.

3.6.3 INCOHERENT SCATTERING

During the under-dense time, accessibility to the whole plasma is good and, as was indicated in the introduction, the scale lengths characteristic of the plasma are in the correct range for collective scattering from the plasma. We will now calculate from the minimum detectable scattered power the minimum possible $S(k,\omega) = \frac{\langle \delta n^2(k,\omega) \rangle}{\bar{n}}$ required.

In backscatter,[35,45] $\frac{dP_s}{d\Omega} = I_i N \sigma S(k,\omega)$ where N is the total number of particles in the scattering volume and $\sigma = 8 \times 10^{-26}$ cm^2, the square of the classical electron radius. After the pinch we have $\bar{n} \simeq 5 \times 10^{17}$/cm^3 and $\Delta V \sim \pi r^2 \ell \sim 0.2$ cm^3 giving $N = 10^{17}$; and as $I_i = 10^7$ w/cm^2, and $\Delta\Omega = 7.5 \times 10^{-3}$ steradian, we find $P_s = 5 \times 10^{-4}$ watts $|S(k,\omega)|$. (The filter

bandwidth $\frac{\Delta\lambda}{\lambda} = 3 \times 10^{-2}$ is sufficiently large to include frequencies up to ω_{pe}, so that $P_s = 5 \times 10^{-4} \int_{-\infty}^{\infty} \frac{d\omega}{2\pi} S(k,\omega) = 5 \times 10^{-4} S(k)$, where $\underline{k} = \underline{k}_s - \underline{k}_i$). Taking into account filter and window loss, and requiring the minimum detectable signal to be $P_s(\text{min.}) \sim$ 1 watt, we need $S(\underline{k}) \geq 2 \times 10^3$.

$S(\underline{k})$ is proportional to the energy in mode $\underline{k}$ and can be calculated in general only for stable plasmas.[35,45] For a thermal plasma $S(\underline{k}) = \frac{1}{2}$ for collective modes, so that the energy in unstable modes must be 4×10^3 over thermal. For a turbulent plasma $S(k)$ shows a resonance near the normal modes: $S(\underline{k}) \propto \frac{1}{|\epsilon(\underline{k},s)|^2}$. Since Re $\epsilon \simeq 0$, $S(k)$ is sensitive to Im ϵ, the mode damping, which is necessarily small in a turbulent plasma. As such, one is best guided by experiment for a practical estimate for $S(k)$. Current-driven turbulence[14] observed in collisionless shocks[14] with crossed $\underline{E}$ and $\underline{B}$ fields has been observed to give $S(k) \simeq 6 \times 10^4$, while beam turbulence[15] has given $10^3 \leq S(k) \leq 10^5$.

The absence of an observable scattered signal in our experiment implies no strong turbulence having $k \simeq \frac{1}{50} R_D$ and $S(k) \geq 2 \times 10^3$ over the <u>whole</u> scattering volume. Instabilities in part of the scattering volume could remain undetected. The absence of strong scattering is surprising in view of the high neutron production in the low-density plasma and the frequently seen nonthermal radiation.

To obtain more condusive evidence, it would be desirable to repeat the experiment with higher laser power and a more

sensitive detector (Cu-Ge detectors at 4.2°K. have sensitivities 10^3 times greater than Au-Ge). It would then be possible to detect scattering from $S(k) \geq$ thermal.

4. DISCUSSION OF DATA

In this chapter we will discuss the data on the radiation emitted from the plasma focus. Before this can be done, we must estimate the average plasma parameters. This will be accomplished through a comparison with Peacock's focus on which the most detailed work has been done to determine n_e, T_e, T_i, etc., the measurements of which are too involved to be repeated for this experiment. Following this we will point out some interesting features of the soft x-ray spectra seen in other experiments which may help interpret our observations.

4.1 FOCUS PLASMA STATE

4.1.1 REVIEW OF THE RELEVANT RESULTS FROM PEACOCK[4,25,31,32]

Peacock's plasma focus is operated at a pinch current of 610 KA. from 42 kJ of stored energy using a solid anode; the filling pressure is 2.5 torr D_2 + 4% Ar. Other characteristics such as geometry, etc., are the same as ours.

The one-nanosecond laser shadowgrams reveal a sharp boundary $\delta\left(\frac{\partial n_e}{\partial r}\right) \leq 1$ mm. between the plasma and magnetic field during the collapse. On arrival at the axis a pinch is formed. The average density of the pinch is $6 \times 10^{18}/cm^3$ with a peak of $4 \times 10^{19}/cm^3$ as determined from an interferogram taken at the beginning of soft x-ray emission. The sharp boundary of the collapse stage gives way to a parabolic density profile in the pinch stage. As the change takes place on times short compared

to magnetic diffusion times, this indicates that some form of anomalous resistivity may exist from the moment the pinch is formed. During the pinch phase $\bar{T}_e$ = 2 keV., as determined from free-bound continuum and satellite/resonance line ratio of He - like Argon ions. From collective light scattering, the deuterium ion temperature T_D is ~ 0.7 keV. The temperature of the Argon ions with $\bar{Z} = 12$ is 9.5 keV. Using these parameters, $\beta = \frac{P}{B^2/8\pi}$ is determined to be $\beta \cong 0.6$. From these values of ion density and temperature only 5% of the emitted neutrons can be accounted for on a thermonuclear basis (i.e., Maxwellian velocity distribution).

From the collective light scattering, $S(\underline{k},\omega)$ for the ion spectrum ($\underline{k}_\perp$ axis) is consistent with $T_e/T_D \cong 3$. Forrest states, "The absolute flux is estimated to be within a factor of three of that expected from a thermal plasma so that gross turbulence during pinch phase can not be present." [31] Recent measurements from other laboratories confirm this result of near thermal $S(\underline{k},\omega)$.[36] However, local regions which may be unstable for times ~ 5 nsec. were revealed in the optical studies.[4]

4.1.2 ESTIMATION OF PLASMA PARAMETER DURING PINCH PHASE

To evaluate our parameters, we used β = 0.6 with our current to get the internal pressure. We assume that the final density is proportional to the filling pressure so that by comparison to Peacock's density we estimate $n_e = 3 \times 10^{18}/cm^3$ for

p = 1.6 torr D_2 + 3% Ar.* (The computer calculation of H.C. Lui gives a pinch compression of 20 over initial filling density giving $n_e = 2.5 \times 10^{18}/cm^3$). As Peacock's results give T_i = 1/3 T_e and $n_e \cong n_i$, then a pressure balance $\beta \frac{B^2}{8\pi} = \sum n_j T_j \cong$ 4/3 $n_e T_e$ gives T_e = 750eV. and T_i =250 eV. where we have assumed a pinch radius r = 1.5 mm. Values for 1.1 torr D_2 + 5% Ar, as well as other characteristic parameters calculated from T_i, T_e, and n_e, are given in table 4-1.

The energy relaxation times t_{DD} and t_{eq} (e-D) for the deuteron-deuteron and electron-deuteron gas and t_{ei}, the electron ion time for momentum transfer (including scattering from Argon ions with $\bar{Z}$ = 10), are calculated by relations given by Spitzer[37]. The absorption length Im. k for transverse electromagnetic wave propagation at 10.6 μm. indicates mild absorption on the plasma scale size. Note that the plasma is sufficiently collisionless, $\omega_{pe}\, t_{ei} \sim 4 \times 10^3$, to allow nonlinear growth to collisionless saturation for instabilities such as the two-stream instability.[38] The values of T_i and n_i give thermonuclear neutron yields[39] of $< 10^5$ whereas the measure yield is $\sim 8 \times 10^8$.

---

* We note that the IR bremsstrahlung measurements at 5.3μ m. gave a ratio of 2.4 for the ratio of emitted power from the DPF at 1.6 torr to that of 1.1 torr. We assume β is the same for both pressures and $\bar{Z}$ of Argon remains constant, then $n_e T_e$ = const. As the bremsstrahlung power goes as $P \propto n_e^2 T_e^{-1/2}$ then $P \propto n_e^{5/2}$. As $(1.6/1.1)^{5/2} = 2.5$, then the emitted bremsstrahlung is consistent with a final density proportional to the filling density.

Table 4-1 APPROXIMATE PINCH PARAMETERS

Pressure	1.6 torr	1.1 torr
$\bar{T}_e$	750 eV.	1.1 keV.
$\bar{T}_i$	250 eV.	370 eV.
$\bar{n}_e$	$3 \times 10^{18}/cm^3$	$2 \times 10^{18}/cm^3$
$\bar{n}_D$	$0.83n_e$	$0.67n_e$
$\bar{n}_{Ar}$	$0.025n_e$	$0.03n_e$
t_{ei}	7×10^{-11} sec.	1×10^{-10}
t_{DD}	4×10^{-9} sec.	2×10^{-8} sec.
t_{eq}(e-D)	2×10^{-8} sec.	8×10^{-7} sec.
ω_{pe}	6×10^{13} rad/sec.	4×10^{13} rad/sec
ω_{ce}	7×10^{12} rad/sec	7×10^{12} rad/sec
Im k (10.6μm.)	$\frac{1}{4}$ cm^{-1}	1/6 cm^{-1}
ω_{pe} t_{ei}	4×10^3	4×10^3

4.1.3 POSSIBILITY OF BEAMS IN THE FOCUS

As was pointed out in the introduction, the neutrons emitted by the plasma focus have anisotropies characteristic of a plasma coexisting with a deuteron beam. Recent measurements[34] made with an 80-m time-of-flight spectrometer have indicated that the ions responsible for the neutrons have a two-velocity distribution. One component is two-dimensional and has an upper limit on the average ion energy of 60 keV, while the second is primarily axial and has an average energy of 300 keV. The techniques used

have not been capable of distinguishing between deuterons produced during the pinch phase or the subsequent low-density stage.

The electron distribution function also has features characteristic of beams. Time-integrated x-ray pinhole photographs (x-rays < 10 keV) show a few (~ 3) small ($r < 0.1$ mm. and $\ell < 0.3$ mm.) x-ray sources located either axially or up to 1 mm. off the axis of the plasma column. The emission perpendicular to the axis $I_\perp$ compared with emission parallel to the axis $I_\parallel$ gives a ratio $\frac{I_\perp}{I_\parallel} \sim 3.5$ for an Argon seeded plasma. Anisotropy of continuum x-ray spectra is produced by a beam of electrons and can account for the observation.[8] As the photographs are time integrated, it cannot be determined whether the sources are produced only during the pinch phase or if they occur in the following low density phase. The fact that these sources are localized indicates that a continuous beam in the axial direction is not responsible and that localized high fields must exist in the focus plasma.

In addition to these x-ray sources, the soft x-ray spectra[41] have a $e^{-h\nu/kT}$ spectrum up to $h\nu \sim$ few kT_e, but for larger photon energies the spectra fail to decrease exponentially. Such spectra are consistent with a tail on the electron distribution.

4.2 DISCUSSION OF THE IR RADIATION

The observed radiation has a spectrum consisting of both thermal and nonthermal emission. The observed nonthermal emission

is dependent on filling pressure and has different characteristics for the high (1.6 torr) and low (1.1 torr) pressure fillings -- although table 4-I gives nearly the same average collision frequency, electron plasma frequency and electron cyclotron frequency during the pinch for both filling pressures. The nonthermal emission exists only during the dense pinch phase for the 1.6 torr data and thus would seem to be dependent on high average density, whereas the nonthermal emission at 1.1 torr actually increases as the density drops at the end of the pinch phase and the power in the nonthermal emission is 10^2 times larger than the nonthermal radiation at 1.6 torr. As such, we will discuss the two separately.

4.2.1 IR DATA FROM 1.6 TORR EXPERIMENTS

As was indicated in chapter 3, with the exception of an occasional short burst of radiation at $\sim 5\mu m$, the emission for $\lambda < 6.5\mu m$ is thermal bremsstrahlung. The dominant source of this radiation is from the high density region of the pinch rather than from the lower density plasma at the end of the pinch column. Recalling our estimates in chapter 3, the volume of the end of the pinch is a few times that of the pinch, but the average density is ~ 5 times higher in the pinch. The thermal bremsstrahlung is $P \propto n_e^2 \Delta V$, indicating that the pinch radiation dominates. Refraction of this end plasma was not a problem for the thermal bremsstrahlung measurements as it was with laser scattering. Since the emission is isotropic, rays may be refracted

into as well as away from the direction of the detector. For $\lambda > 6.5\mu m.$ nonthermal emission is observed. The following statements can be made about this radiation;

A) The emission is observed: $6.5\mu m. < \lambda < 9\mu m.$ (3×10^{14} rad/sec $> \omega >$ 2×10^{14} rad/sec).

B) Though most of the measurements in this band show some enhancement, an enhancement of 10 times thermal is rare (only 3 out of 26 observations).

C) The enhanced radiation is observed during the dense pinch but decays faster than the thermal emission (see figure 3-7).

D) During the pinch the cyclotron frequency is too low to be related to emission: $\frac{\omega}{\omega_{ce}} \sim 25$.

E) As $2\ \omega_{pe} = 1.2 \times 10^{14}$ rad/sec associated with the average density is too low to equal the frequency of nonthermal radiation, the radiation must be generated in the central region where n_e may be as high as $5\ \bar{n}_e$.

F) The maximum enhancement is ~ 100 but the increase in emissivity per volume is larger than 100 since less than the total pinch volume participates in the emission.

Only the plasma frequency is close to the emitted frequency, which indicates that the enhanced radiation is a result of plasma oscillation. To aid further discussion of the data, we will outline some important information concerning the relation of plasma oscillations to bremsstrahlung.

It is assumed that the same electrons responsible for the nonthermal soft x-ray spectra are also responsible for the excitation of plasma oscillation. It is not clear whether these oscillations are excited by beams of electrons or from the non-Maxwellian

electrons on the tail,or both.

If a beam exists on the tail of a Maxwellian, then the distribution function is no longer monotonically decreasing and the plasma is unstable against growth of plasma oscillation.[42] This is a result of the change in sign of the Landau damping $\gamma = -\frac{\pi}{2} \frac{\omega_{pe}^3}{k^2} F'\left(\frac{\omega}{k}\right)$ where $F(u) = \int_{-\infty}^{\infty} d\underline{V}\, \delta\left(u - \frac{\underline{k}\cdot\underline{v}}{\underline{k}}\right) f_e(\underline{v})$ and $f_e(\underline{v})$ is the electron distribution function. Waves may grow coherently with the beam until non-linear effects diminish the growth rate (i.e., $F'\left(\frac{\omega}{k}\right) \longrightarrow 0$). The system further evolves by interaction of the waves with the distribution function to produce a final state of a near-Maxwellian with a broad tail with energies up to several times the initial beam energy.[43,44] Evidence for a beam and the final state of a beam plasma interaction has been indicated previously.

A tail on the distribution could also be formed directly by acceleration of particles out of the distribution function by the high electric fields which are either applied by the electrical circuit or generated of MHD instabilities.

The presence of a tail on the distribution guarantees some enhancement of plasma oscillations. The increase of particles with $V > \overline{V}_e$ results in an increase of plasma waves through Čerenkov radiation while the decrease in $F'\left(\frac{\omega}{k}\right)$ results in decreased damping. However, a Maxwellian with a tail is a stable distribution and as such will not have the high level of plasma oscillations that is produced by a beam plasma interaction.

Once plasma oscillations are generated, they must couple

to transverse waves in order to propagate outside the plasma. Such coupling[45] can result from macroscopic effects such as anisotropy or density gradients, and leads to radiation at the frequency of the plasma waves $\omega = \sqrt{\omega_{pe}^2 + k^2 \overline{V}_e^2} \leq 1.4\ \omega_{pe}$. Transverse waves may also be generated by scattering of plasma waves within the volume.[46,47] These waves may scatter from low frequency fluctuations or waves (e.g., in acoustic), which results in emission at the plasma wave frequency. Or, they may scatter from high frequency thermal electron plasma fluctuations or nonthermal electron plasma waves, which results in emission at $2\omega \leq 2.8\ \omega_{pe}$.

To determine which mechanism might be responsible, we must rely principally on the frequency of the emitted radiation. Since the scale of the gradient is ~ 1 mm. (whereas plasma waves have $\lambda > \lambda_D \sim 10^{-1}\mu$m.), we assume that boundary effects cannot be the dominant coupling mechanism. Under such circumstances, the nonthermal radiation always has a two-band structure[45,48] of ω_{pe} and $2\omega_{pe}$ both significantly enhanced. (Radiation at $3\omega_{pe}$ is not observed). No frequency corresponding to twice the frequency of observed nonthermal emission was observed during its emission time. If the observed frequency is ω_{pe}, then the corresponding density is $n_e = 1.2 \times 10^{19}/\text{cm}^3$. From Peacock's interferogram we see that the maximum density is $n_e \sim 5\bar{n}_e$. Such a high density may exist in a small fraction ($\sim 10^{-4}$) of the total pinch volume. It seems unlikely that no adjacent region of larger volume would fail to yield enhanced emission. As such, we propose that the emission is $2\omega_{pe}$ radiation. However, the question of whether the

emission is ω_{pe} or $2\omega_{pe}$ is open until measurements are made with two harmonically related detectors with capabilities to 20 μm. or until ruby laser scattering is done to detect the electron plasma frequency satellite.

It is clear that the emitting volume is a fraction of the total pinch volume. The observed band of nonthermal emission corresponds to plasma waves of frequency ω with $\omega_{pe} < \omega < 1.4\omega_{pe}$. This would allow for a maximum variation in density of 2 ($\omega_{pe} \propto \sqrt{n_e}$). As the bandwidth for the homogeneous medium is also $\omega_{pe} < \omega < 1.4\omega_{pe}$ ($\omega = \sqrt{\omega_{pe}^2 + k^2\overline{v}_e^2}$ with $o < k < \frac{kD}{2}$), the bandwidth broadening due to the inhomogenity of n_e is not great.

The enhancement of $2\omega_{pe}$ radiation is sensitive to the distribution of waves in $\underline{k}$ space. Since the waves must satisfy the relations of conservation of energy and momentum, $\omega(k_T) = \omega(k) + \omega(k')$ and $\underline{k}_T = \underline{k} + \underline{k}'$, where k_T and $k,(k')$ refer to the transverse wave and plasma wave (longitudinal) wave vectors respectively. As $\omega(k_T) \cong 2\omega_{pe}$, the dispersion relation for transverse waves $[\omega(k_T)]^2 = \omega_{pe}^2 + k^2c^2$ gives $k_T \cong \sqrt{3}\,\frac{\omega_{pe}}{c}$. As k and k' $\sim \frac{\omega_{pe}}{v}$, where v is the velocity of the Čerenkov emitting electron, and v is a few times $\overline{V}_e$, we need $\underline{k} + \underline{k}' \cong 0$ since $\overline{V}_e \ll c$. Thus, the conversion of two longitudinal plasma waves into a transverse wave can occur only if two waves collide "head-on". If a beam excites the waves, then they have the beam as a preferred direction. We assume that in a finite medium, waves are easily randomized due to reflection from the boundaries and, therefore, the emission is isotropic.

Calculations of Tidman and Dupree [46] for a stable distribution function give enhancement of $2\omega_{pe}$ radiation as:

$$j(2\omega_{pe}) \cong \frac{e^2 \omega_{pe}^2 K^2 \sqrt{3}}{15\pi^2 c^2} \int_0^{k_D} dk \left\{ \frac{F_e(\omega/k)}{F'(\omega/k)} \right\}^2 , \text{ where}$$

j is the plasma emissivity,

$\frac{\omega_{pe} m}{4\pi^2} \int_0^{k_D} k\,dk \left(\frac{F_e(\omega/k)}{F'\ \omega/k}\right)$ is just the energy in the plasma waves and K is the transverse wave vector. The emission formula shows the expected quadratic dependence on the energy in the plasma wave. As can be seen, the emission is very sensitive to the shape of the tail of the distribution function and will show greatest enhancement for $F'(\omega/k) \longrightarrow 0$. The integral has been evaluated for a distribution function consisting of a Maxwellian having $\frac{T_e}{m} = \overline{V}_e^2$ combined with a second Maxwellian of lower density but higher temperature $\frac{T_E}{m} = \overline{V}_E^2$ which forms the tail. The resulting enhancement over thermal emission is:

$$\frac{j(2\omega_{pe})}{j(\text{thermal})} \propto \left(\frac{V_E}{V_e}\right)^4 .$$

As soft x-rays show departure from Maxwellian beyond a few times T_e, we might take $V_E^2 = 10\ V_e^2$, which gives an enhancement of 100. This enhancement appears too low, to account for the maximum enhancement since the emission apparently comes from less than the total volume. It is more probable that an instability drives the plasma oscillation to a higher level during the largest enhancements.

In addition to the enhancement lasting the major portion of the pinch duration, a short burst of radiation enhanced ~ 4 times thermal is occasionally observed at ~ 5 μm at the time the pinch breaks up. Such an increase in frequency may be due to a density increase as the pinch column constricts or possibly to a change in plasma refractivity as the pinch breaks up and thus increases the visibility of the central core.

4.2.2 IR DATA FROM 1.1 TORR EXPERIMENTS

It is observed that a 50% change in pressure produces a radically different nonthermal radiation (see figure 3-10). The thermal bremsstrahlung at 5.3μ has an identical time development for both 1.6 and 1.1 torr data, and the difference in amplitude of emission can be accounted for by the difference in density and temperature of the pinch. The frequency of the observed nonthermal radiation does not follow the density associated with the pinch; indeed, the radiation is most intense after the dense pinch phase is over.

After the density has dropped, there is still emission of soft x-rays and neutrons as well as interaction of 10.6 μm laser with the plasma. Since the frequency of nonthermal radiation is now larger than ω_{pe}, $\frac{\omega}{\omega_{pe}} \sim 4$, one might speculate that the cyclotron harmonic radiation from mildly relativistic electrons is responsible for the radiation. The electron cyclotron frequency is $\leq 7 \times 10^{12}$ rad/sec assuming the channel for the total current is no smaller than that of the original pinch. The observed radiation

frequency is 1.8×10^{14} rad/sec implying that the harmonic number ~ 25. However, harmonic radiation would appear over a broad band from ω_{ce} to beyond the observed frequency since the radiation is $\sim 10^6$ over thermal. No enhanced radiation was observed for $\lambda < 7\,\mu m$; there was only one enhancement at 7μ in 36 measurements for $\lambda < 10.6\,\mu m$. If we rule out cyclotron harmonic radiation, we are forced to conclude that local regions are produced by the current which contains compressed plasma so that the plasma frequency is near the observed frequency.

Since these regions do not show up in the thermal spectrum -- nor have they yet been observed in published optical data -- they must be much smaller than the original pinch. If we construct a filamentary plasmoid of $n_e = 5 \times 10^{18}/cm^3$, radius of 100μ, $T_e = 1$ keV (characteristic of the pinch plasma) and $\beta = \frac{1}{2}$, then $\beta \frac{B^2}{8\pi} = n k T$, gives $B = 3 \times 10^5$ gauss corresponding to a filament current of $\sim 10^4$ amperes, which is a small fraction of the total current. We have chosen n_e so that the radiation corresponds to $2\,\omega_{pe}$ as no nonthermal radiation was observed at $5.3\,\mu m$. Other radii could be chosen, but they would be limited to a size not much larger than 300 μm, at which point their thermal emission could be observed. Filaments much smaller than 100 μm. would not remain intact against resistive diffusion. For a filament of $r = 100\,\mu m$ the resistive diffusion time[49] $\tau = \frac{4\pi\sigma r^2}{c^2} \sim 100$ nsec. with $\sigma = \frac{n_e e^2}{m \nu_{ei}}$ calculated for classical ν_{ei} at $T_e = 1$ keV. Actually, the conductivity may be lower due to the enhanced fluctuation.

The emission from a plasmoid, as seen in figure 3-10, may actually consist of bursts, since the detector rise time is $\sim$ 30 nsec. By comparing the burst of enhanced emission at 5 μm. in figure 3-7 where the rise time is also 30 nsec. to that of figure 3-9 where the rise time is 7 nsec., the effect of detector rise time is clearly seen. A short lived filament is more reasonable in view of its questionable MHD stability and rapid magnetic diffusion.

As has been indicated, local x-ray sources about the same size as this plasmoid, have been seen in Bostick's x-ray photographs.[8] Recent data has shown that the time resolved soft x-ray emission also shows a series of sharp spikes ($\sim$ 4) of $\sim$ 30 nsec. duration.[50] However, it is not yet clear if these spikes correlate with the x-ray sources. Although the x-ray sources may not be the same as the plasmoid postulated here, they show that local phenomena, which are not characteristic of the bulk of the plasma, do occur in the plasma focus.

We ask if such a small region could radiate sufficient power based on conservation of energy only. Assuming the enhanced radiation is isotropic, then this total power, assuming a 1 μm bandwidth, is

$$P \cong 100 \text{ watts } \frac{1\ \mu m}{\Delta \lambda} \quad \frac{4\pi}{\Delta \Omega} = 5 \times 10^{-4} \text{ J/nsec.}$$

The total radiation over the rest of the spectrum for $n_e = 10^{19}$, T_e = 1 keV., D_2 + 3% Ar, including line radiations is given by Peacock[51] as

$$P = 10 \text{ J/nsec. cm}^3 \quad \Delta V \cong 10^{-3} \text{ J/nsec.}$$

We see that almost as much power is radiated from conversion of plasma oscillation as due to bremsstrahlung, recombination and line radiation over the rest of the spectrum. As the Argon ion increases the radiation by $\sim 10^2$ over pure D_2, the radiation of a D_2 plasma would be completely dominated by the nonthermal emission. The power dissipated in this volume by classical resistivity is

$$P = j^2 \eta \Delta V \cong 4 \times 10^{-2} \text{ J/nsec.}$$

which is sufficient to account for the energy source. With additional power going into plasma waves, the resistivity might even be higher.

4.3 CONCLUSION

As the plasma focus is a source of a nonthermal neutron and x-ray spectra and produces more neutrons than can be accounted for on a thermonuclear basis, it is logical to postulate turbulence as an explanation. In these experiments we proposed to search for turbulence through collective laser scattering and bremsstrahlung emission. At the outset we had little idea as to which experiments would yield results.

Bremsstrahlung emission yielded the greatest amount of information. In contrast to the visible emission, the IR thermal bremsstrahlung (see figure 3.10) provided information on plasma density. This density information demonstrated a lack of correlation between density and neutron yield. It was essential for the interpretation of the nonthermal emission observed at

longer wavelengths.

The nonthermal emission is often too large to be consistent with a high electron velocity tail on a Maxwellian, particularly in the example of the 1.1 torr data where enhancements go as high as 10^6 over thermal, and it must be caused by turbulent levels of plasma oscillation (see figures 3.7 and 3.10). During the pinch phase the resulting emission comes not from the whole pinch but from a smaller volume near maximum density. This demonstrates the local nature of the instability. Further evidence for local instabilities comes from the nonthermal emission during the fall in density and subsequent low-density stage of the discharge. The best interpretation is that plasmoids form and produce energetic plasma with density an order of magnitude higher than the plasma from which they are formed. It is believed that this is the first time that such phenomena have been observed. The formation of these plasmoids indicates that the current does not flow uniformly. This could be expected if plasma is turbulent and more resistive than a thermal plasma.

The laser backscatter experiments did not yield positive results. This is quite consistent with the assumption that instabilities occur in local regions as shown by the nonthermal emission. The forward refracted signal, however, does give an indication of an abrupt drop in density after the pinch. This signal was always observed at 1.1 and 0.9 torr, but usually not observed at 1.6 torr; this suggests that the deflection was produced by the same turbulence which caused the production of plasmoids.

Interesting plasma turbulence has been discovered by this work and clearly more research might be done. To obtain sufficient understanding of the radiation, one would need to use two harmonically related detectors and extend the measurements to longer wavelengths. If plasmoids form with $n_e \sim 5 \times 10^{18}/cm^3$, they presumably form with lower density too; this would be revealed by examining the spectrum at longer wavelengths. In addition the spatial radiation pattern would help determine the source of the radiation.

Another laser scattering experiment using higher laser power at 10.6μ coupled with a more sensitive detector may yet yield positive results. An examination of the forward signal could determine whether the beam is deflected by fluctuations or a density gradient. Ruby scattering would be particularly useful as the frequency is well removed from that of nonthermal emission. Furthermore, the high frequency would permit penetration of the laser beam into the dense pinch so that scattering from electron fluctuations could be accomplished without the refractive loss.

APPENDIX

CO_2 TEA LASER

Much work has gone into developing TEA Lasers since Beaulieu[29] first reported successful operation in 1970. The laser has two important features: high theoretical efficiencies for CO_2 lasing, and high energy density by virtue of operating at atmospheric pressure.

Early lasers used large numbers of resistors to limit the discharge current and prevent arcs. Even with this procedure, however, the discharge is far from uniform. Two improved discharge methods have been discussed in the literature.[52,53] Both use corona discharge as a source of free electrons to create a uniform discharge between parallel electrodes but differ principally in the shape of the electrodes. We constructed the type described by Yu-Li Pan as the electrodes are simpler to fabricate than the Rogowski profile electrodes described by Seguin. The electrode cross section with its corona discharge wires is shown in figure A-1. The only difficulty is to keep the wires even with the top of the groove. If recessed into the groove, a discharge could be maintained which appears uniform to the eye but did not produce a lasing discharge! Raising the wires to the edge of the grooves did, presumably due to a large supply of electrons from the corona. The electrodes were 68 cm. long, and were located in a $2\frac{1}{2}$ in. diameter plexiglass tube closed off at both ends with NaCl Brewster windows.

The discharge circuit can be seen in fig. A-2 along with the resulting current and voltage pulses. The circuit differs from a straight capacitive discharge by the L.C. combination which serves to limit the rate of rise of the voltage across the electrodes so that the corona discharge can build up. When the output voltage reaches sufficient amplitude, the discharge starts. The charge on C_1 accounts for large initial pulse of current whereas L_1 causes the discharge voltage to drop after the initial current so that an arc will not form after the lag period.

The laser mixture was normally He: CO_2: N_2 of 8:1:1 which gave 1 MW and a pulse half width of 150 nsec. Higher power could be obtained by using a richer mixture, He:CO_2:N_2 of 5:1.5:1, with a peak power of 5 MW and half width of 100 nsec.

The cavity consisted of a flat Ge mirror (65% reflecting) and a gold-coated total reflector of radius 2 m, both 5/8" Dia. The mirrors and discharge chamber were mounted on an Al I-beam. As Ge does not transmit in the visible, auto collimation can not be used to align the laser. Instead the laser was aligned by introducing a HeNe beam into the laser cavity with a microscopic slide cover as a beam splitter. The slide cover is thin enough (50μ) so that there is negligible beam displacement. The mirrors are then adjusted to send the red beam back and forth on itself. After one gets accustomed to this procedure it is easy to line up an IR laser as precision is not important at these long wavelengths and high gain mixture.

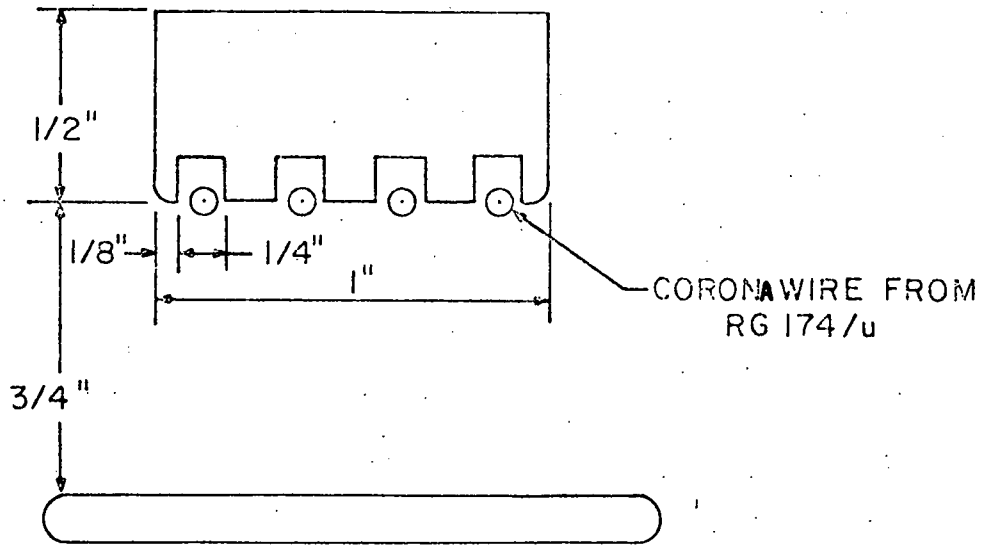

Figure A.1 Cross sectional drawing showing dimensions and the relative positions of electrodes and corona wires.

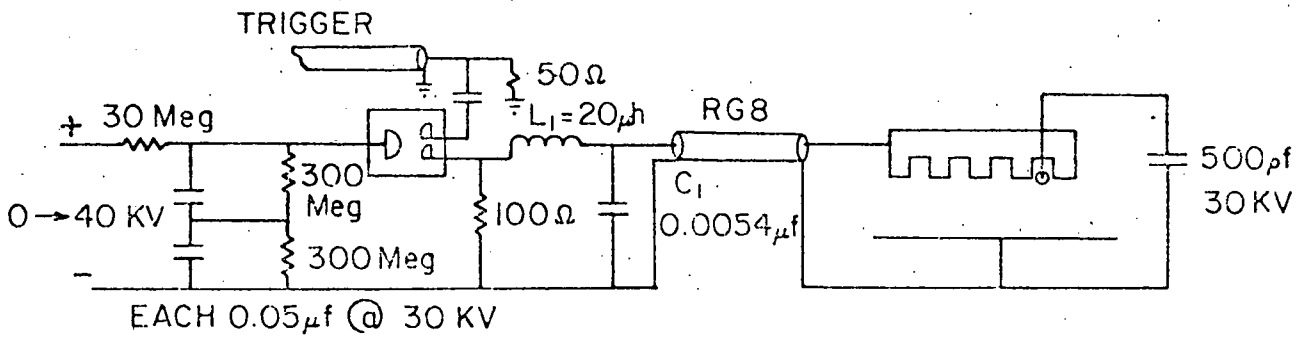

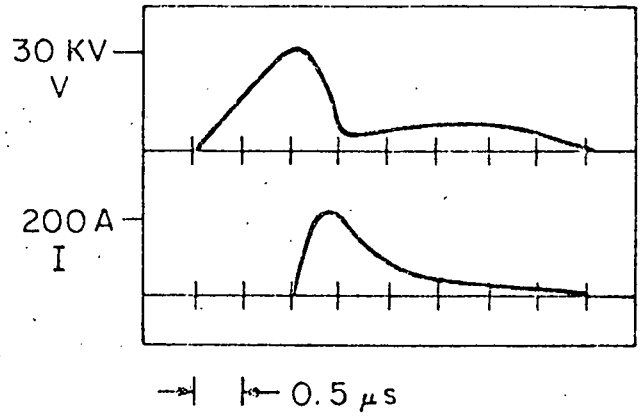

Figure A.2 Schematic of laser discharge circuit along with current and voltage wave forms measured at the electrodes.

REFERENCES

1. MATHER, J.W., in GRIEM, H.A., and LOVEBERG, R.H., Methods of Experimental Physics, Vol. 9, part A, Academic Press, (1970).

2. FILIPPOV, N.V. et al., Nucl. Fusion Suppl. 2, 577, (1962).

3. POTTER, D.E., Phys. Fluids 14, 1911, (1971).

4. PEACOCK, N.J., HOBBY, M.G., and MORGON, P.D., Proc. 4th Conf. Plasma Physics and Controlled Nuclear Fusion Research Madison CN-28/D-5 (International Atomic Energy Agency, Vienna, (1972))

5. BERNSTEIN, M.J., MESKAN, D.A., and VAN PAASEN, H.L.L., Phys. Fluids 12, 2193, (1969).

6. JALUFHA, N.W. and LEE, JA. H., Phys. Fluids 15, 1954, (1972).

7. VAN PAASEN, H.L.L., VANDRE, R.H., and WHITE, R.S., Phys. Fluids 13, 2606, (1970).

8. BOSTICK, W.H., NARDI, V., and PRIOR, W., J. Plasma Phys. 8, 7, (1972).

9. TIDMAN, D.A., DUPREE, T.H., Phys. Fluids 8, 1860, (1965).

10. DAWSON, J.M., Advances in Plasma Physics, Vol. 1 , (Interscience 1968).

11. WILD, J.D., SMERD, S.F., and WEISS, A.A., Ann. Rev. Astron. Astrophysics 1, 291, (1963).

12. PERKINS, F., and SALPETER, E.E., Phys. Rev. 139A, 55, (1965).

13. APEL, J.R., Phys. Fluids, 12 , 291, (1969).

14. MAISSONNIER, CH., PECORELLA, F., RAGER, J.P., SAMUELLI, M., Second Topical Conf. on Pulsed High-Beta Plasmas, Garching, (1972).

15. KORNHERR, M., DECKER, G., KEILHACHER, M., LINDENBERGER, F., and ROHR, H., Phys. Letters 39A, 95, (1972).

16. DAUGHNEY, C.C., HOLMES, L.S., and PAUL, J.W.M., Phys. Rev. Lett. 25 , 497, (1970).

17. BERNARD, A., Private communication.

18. PRIOR, W., Private communication.

19. TOEPFER, A.J., SMITH, D.R., and BECKNER, E.H., Phys. Fluids 14, 52, (1971).

20. CARPENTER, J.P., WARE, K.D., BOTTOMS, P.J., WILLIAMS, A.H., and MATHER, J.W., Proc. Eng. Problems of Fusion Research, Los Alamos, (1969), LA - 2450.

21. HAARMAN, R.A., Proc. Eng. Problems of Fusion Research, Los Alamos, (1969), LA - 2450.

22. ENGE, H.A., Introduction to Nuclear Physics, Addison-Wesley, (1966).

23. OSHER, J.E., in HUDDLESTONE, R.H. and LEONARD, S.L., Plasma Diagnostic Techniques, Academic Press, (1965).

24. BERNSTEIN, M.J., Rev. Sci. Inst. 43, 1323, (1972).

25. PEACOCK, N.J., SPEER, R.J., and HOBBY, M.G., Culham Laboratory Report, CLM-P197.

26. _____, RCA Photomultiplier Manual, RCA Harrison, N.J., (1970).

27. LANTER, R.T., and BONNERMAN, D.E., Los Alamos Scientific Laboratory Report, LA - 3488 - MS, (1966).

28. KRUSE, P.W., MC-GLAUCHLIN, L.D., and MCQUISTAN, R.B., Elements of Infrared Technology: Generation Transmission and Detection, Wiley, (1962).

29. BEAULIEU, J.A., Proc. IEEE 59, 667, (1971).

31. FORREST, M.J., Culham Laboratory Report, CLM-PR15 B.21, (1972).

32. MORGAN, P.D. and PEACOCK, N.J., Proc. Second Topical Conf. on Pulsed High-Beta Plasma E-9, Garching, (1972).

33. RUSBRIDGE, M.G., Plasma Physics 10, 95, (1968).

34. WORT, D.J.H., Plasma Physics 8, 79, (1966).

35. SITENKO, A.G., Electromagnetic Fluctuations in Plasma, Academic Press, (1967).

36. EISNER, M., DOWNING, J.N., and MATHER, J., Bull. Am. Phy. Soc., 1023, (1972).

37. SPITZER, L., JR., Physics of Fully Ionized Gases, Interscience, (1962).

38. GULA, W.P., Thesis, Columbia University, (1972).

39. D'YACHENKO, V.F., and IMSHENNIK, in LEONTOVICH, M.A., Reviews of Plasma Physics, Vol. 5., Consultants Bureau, (1970).

40. CONRADS, H., CLOTH, P., DEMMELER, M., and HECHER, R., Phys. Fluids 15, 209, (1972).

41. MATHER, J.W., BOTTOMS, P.J., CARPENTER, J.P., WARE, K.D., and WILLIAMS, A.H., Conf. Plasma Phy. and Controlled Nuclear Fusion Research, Wisconsin, CN-28/D-5, (1971).

42. JACKSON, J. D., J. Nuclear Energy, part e, 1, 5, (1960).

43. DAWSON, J.M., and SHANNY, R., Phys. Fluids 11, 1506, (1968).

44. DUM, C.T., and SUDAN, R.N., Phys. Fluids 14, 414, (1971).

45. BEKEFI, G., Radiation Processes in Plasmas, John Wiley, N.Y., (1966).

46. TIDMAN, D.A., and DUPRESS, T.H., Phys. Fluids 8, 1860, (1965).

47. TSYTOVICH, V.N., Nonlinear Effects in Plasma, Plenum Press, (1970).

48. CHIN-FATT, C., and GRIEM, H.R., Phy. Rev. Lett. 25, 1644, (1970).

49. JACKSON, J.D., Classical Electrodynamics, John Wiley, (1962).

50. PRIOR, W., private communications.

51. PEACOCK, N.J., WILCOCK, P.D., SPEER, R.J., and MORGAN, P.D., Plasma Physics and Controlled Nuclear Fusion Research, Vol. II, 51, International Atomic Energy Agency Vienna, (1969).

52. SEGUIN, H.J., MANES, K., and TULIP, J., Rev. Sci. Inst. 43, 1134, (1972).

53. PAN, Y.L., BERNHARDT, A.F., and SIMPSON, J.R., Rev. Sci. Inst. 43, 662, (1972).